PLASMA GENERATOR CHARACTERISTICS

AND RELATED HEAT TRANSFER STUDIES

THE CHARACTERISTICS OF A PLASMA GENERATOR WITH A
TRANSPIRATION-COOLED POROUS ELECTRODE AND
THE MEASUREMENT OF BULK HEAT TRANSFER FROM THE
HIGH TEMPERATURE GAS HEATED BY THE PLASMA ARC

By

JACK SHIU-KAU LI, B.A.Sc.

A Thesis
Submitted to the Faculty of Graduate Studies
in Partial Fulfilment of the Requirements
for the Degree
Master of Engineering

McMaster University

May 1964

MASTER OF ENGINEERING (1964)
(Mechanical Engineering)

McMASTER UNIVERSITY
Hamilton, Ontario.

TITLE: The Characteristics of a Plasma Generator with a Transpiration-Cooled Porous Electrode and the Measurement of Bulk Heat Transfer from the High Temperature Gas Heated by the Plasma Arc

AUTHOR: Jack Shiu-kau Li, B.A.Sc. (University of British Columbia)

SUPERVISOR: Doctor J. H. T. Wade

NUMBER OF PAGES: viii, 101

SCOPE AND CONTENTS:

The report describes an experimental study of the performance characteristics of the plasma generator and the bulk heat transfer measurements from a high temperature gas after leaving the plasma arc.

Preliminary tests on the original plasma generator as designed by D. Male, Mechanical Engineering class of 1961-62, indicated arc instability at high gas flow rates and a high erosion rate of the cathode. By reversing the polarity and introducing a water-cooled copper anode combined with a transpiration-cooled porous cathode, the arc stability was improved and the erosion rate of the cathode reduced. The performance characteristics of the new design were studied, with the plasma generator operating under an electric field potential of 18 - 25 volts, field current 70 - 100 amperes and a transpiration fluid flow of 80 - 200 gm./min.

The heat transfer phenomenon from the high temperature gas was studied using a parallel-cocurrent-flow, tube-and-shell heat

exchanger. The heat exchanger was instrumented to permit measurement of the longitudinal temperature variations of the cooling water, the tube wall and the hot gas stream. A heat transfer analysis was then carried out with the necessary corrections applied to account for the temperature measurement techniques and the variations in physical properties of the hot gas.

ACKNOWLEDGEMENTS

The author wishes to thank Dr. J. H. T. Wade for his constant encouragement, guidance and generous help in initiating, planning and completing the experiment.

The contribution of D. Male, Mechanical Engineering 1962 class, to the original design of the plasma generator is gratefully acknowledged.

The experiment was financially supported by the Department of Mechanical Engineering at McMaster University.

TABLE OF CONTENTS

TEXT

LIST OF FIGURES

TEXT

1. INTRODUCTION

The development of heating a gas with an electric arc to very high temperatures has been under extensive study during the last few years. Its importance has emerged with the rapid advances in the application of magnetohydrodynamics to direct power conversion and in space technology. The space problems often encountered include the simulation of the hypersonic and hyperthermal re-entry conditions and the need for outer-space propulsion techniques.

As an initial step in future study of some of the problems in direct power conversion in the Mechanical Engineering Laboratory at McMaster University, preliminary experiments were carried out on the original plasma generator as designed by D. Male. Arc instability and a high erosion rate of the cathode were indicated. Subsequently the electrode configuration was modified. Also as a logical step to further studies of high temperature stagnation heat transfer, the convection heat transfer phenomenon of the hot gas was investigated.

The first part of this report describes an experimental study of the performance characteristics of the plasma generator with a transpiration-cooled porous cathode and a water-cooled copper anode. The characteristics included the influence of the electric field potential between 18 - 25 volts, a field current of 70 - 100 amperes and a gas flow rate of 80 - 200 gm./min. upon each other. The energy transfer efficiency of the generator was examined at different power inputs by measuring the energy losses to the cathode and anode holders. The temperature of the plasma arc was estimated with the aid of Saha's equation.

For the heat transfer study, the high temperature subsonic gas jet was allowed to emerge into a parallel-cocurrent-flow, tube-and-shell heat exchanger. The longitudinal temperature variations of the cooling water, the tube wall and the hot gas were measured with appropriate thermocouples. Based on these measurements, the heat transfer phenomenon from the hot gas to the cold wall was analysed. The experimental conditions included large temperature differences, low velocity of the hot fluid, and significant changes of the physical properties of the gas as a function of temperature.

2. LITERATURE REVIEW

The engineering application of the electric arc for heating gases to very high temperatures starts from the beginning of the century. However, the lack of need for high temperatures discouraged many early workers. Since 1955, the urgent need for a device to produce high temperatures and high gas velocities in re-entry simulation studies has resulted in rapid development of arc plasma generation technology. At the same time plasma generation opens a new field in metal cutting and spraying; and in recent years it forms the basis of other specific fields including space propulsion and probably most important the direct power conversion of heat to electricity.

The theory behind the electrical discharges in gases at high and low pressures has been well-established in many physics textbooks and technical journals (for example, by Langmuir (1)[+], by Sommerville (2) and by Francis (3)). Based on the theory of the electrical discharges in gases, the principles of the arc phenomena and plasma generation were developed many years ago.

It might be said that up to 1955, in Germany, considerable amount of work has been done in the science of arc plasma. In 1909 O. Schoenherr started experiments on gas-stabilized carbon arc. In 1929, H. Gerdien and A. Lotz announced their successes in high intensity

[+]Numbers in brackets designate References at end of paper.

water-vortex stabilized arc. In the early 1950's Maecker, Weiss (4) and Peters worked on the arc device as proposed by H. Gerdien and A. Lotz, while Finkelnburg and his co-workers studied on the unconfined high intensity carbon arc. In 1954, Maecker and Finkelnburg reviewed the accomplishments of the previous work in arc physics, and laid down the fundamentals of the state of knowledge in arc plasma, as of 1954. Their article (5) also included the descriptions of various plasma generator configurations. Much of the recent development from 1955 onward has been carried out in the United States, where a number of organizations are developing new designs in plasma generator in various applications. To briefly mention a few of these organizations and their research fields, we have the following: Stoke and Knipe of Temple University, Philips and Ferguson of Stanford Research Institute in chemical synthesis; Giannini, Ducati, van Jaskowsky, Ragusa, Blackman of Plasmadyne Corp. in refractory processing; Vitro Laboratories, Avco Lab., Chicago Midway Lab, General Electric Lab, NASA-Langley, NASA-Ames, etc. in re-entry simulation problems and magnetohydrodynamic power generation (6), (7).

Reviewing various types of plasma generators, it is found that practically all of them have two common features: (i) the electrodes have a common central axis, (ii) the gas flows through the gap between the electrodes, in order that most of the gas can be heated by the electric arc. The common electrode materials are carbon, water-cooled copper and thoriated tungsten. The usual gas medium includes air, argon, helium, hydrogen, oxygen, and nitrogen. The final choice of the electrode material, configurations, gas medium and power input to the arc depends on the field of application.

Eckert and Schoeck of the University of Minnesota (8) reported their experiments on the transpiration-cooled anode of an electric arc. A porous graphite anode was used to permit the transpiration process of the fluid (argon). In this way, the anode was adequately cooled and the erosion of the anode was negligible. At the same time the transpiration fluid was heated to high temperatures when passing through the anode fall space, and the arc column. Eventually the fluid emerged as a hot plasma jet. The dependence of the arc voltage upon the mass flow rate of the transpiration fluid was studied for currents between 100 and 200 amperes.

C. Sheer and his co-workers at Vitro Laboratories however, were considered to be among the first group who investigated the arc phenomenon accompanying the transpiration-cooled anode. In 1961, Sheer, Cooney, Rothacker and Sileo (9) published a detailed report on energy exchange in the high intensity arc plasma. The paper not only gives a good review of the pertinent arc phenomena, but also the rationale of fluid transpiration through porous electrodes. An analysis was made on the pore size criterion, energy partition in the anode fall space and energy sinks for a porous anode. Experimental studies on the performance characteristics were carried out using a porous graphite anode, and a carbon disk-cathode with a power input between 2.80 kw. and 6.70 kw. and an argon gas flow rate of 79 - 478 gm./min., giving an energy transfer efficiency of 70.5 - 80.9%.

The plasma generator as described in the present report was originally designed by D. Male during his fourth year in Mechanical

Engineering at McMaster University. The electrode configuration was based on the work of Sheer, and his co-workers.

The stability of the arc process depends not only on the electrode configuration but also on the polarity and gas flow rates. In a transpiration-cooled electrode assembly where the two electrodes are axially located along the gas path, the stability of the arc is to a great extent a function of the polarity.

The effect of reversed polarity in arc plasma generation has received some study. Dooley, McGregor and Brewer (10) reported such phenomena on Gerdien-type plasma generator (using water vapor as the working fluid). With forward polarity, i.e, the anode-cathode configuration in which the anode is upstream of the cathode the action of the fluid flow forced the arc downstream farther than normal. As a result of the increase in the arc length, the arc became unstable and finally extinguished itself. With backward polarity, i.e., cathode-anode, a stable flame even at high fluid flow rates was obtained. It has been observed that freedom from blown arcs would provide a necessary but not sufficient condition for equilibrium.

High temperature heat transfer processes have been studied by a number of people. M. Perlmutter and R. Siegel (11) have made an analysis on high-temperature heat-transfer processes from a hot tube wall to the cool gas passing through it, accounting for the effects of forced convection and radiation. Zellnick and Churchill (12) studied the convective heat transfer phenomena from high temperature air in a tube. Many others (13, 14, 15, 16) have dealt with similar problems. Yet not many reports are found on heat transfer from high temperature gas emerging from a plasma jet.

Experiments on anode heat transfer have been reported by various people. Wilkinson and Milner (17) divided a copper anode into several zones, measuring the energy transfer to each zone separately. In this way, a local distribution of the heat transfer intensity to the anode was obtained. However, the current intensity at the anode was not measured, the local energy transfer by the electrons could not be calculated. On the other hand, Nestor (18) performed an experimental determination of the current density and heat transfer intensity distribution at the anode of high current arcs in inert gas medium, while Schoeck (19) presented a detailed investigation on the physical phenomena involved in anode heat transfer for high intensity arcs.

Emmons of Harvard University (20) reviews the recent developments in plasma heat transfer. The first part of the paper discusses the fundamentals in plasma dynamics, and the rest is devoted to the methods of determining the physical properties of the common arc fluids at extremely high temperatures (up to $50{,}000^{\circ}$k) and at various pressures (0.1 to 100 atm.)

Stagnation heat transfer at high temperatures was investigated by Stokes, Knipe and Streng (21). The transient heat transfer rates from an argon plasma jet to a small water-cooled copper heat probe were obtained up to 4.5 k cal./cm^{2}sec. (3,770,000 BTU/hr.ft^2). The stagnation heat transfer phenomena were also studied by Reed (22) who used induction plasma flames and oxy-hydrogen flames as the heat sources. The surface probe consisted of a copper face .0625 inch thick and two five inch square sections separated by a 0.03125 inch sheet of teflon. Heat transfer intensities up to 145 watts/cm^2

(317,000 BTU/hr.ft^2) were obtained with oxygen-hydrogen burners.

Wethern and Brodkey of Ohio State University (23) recently published a paper on heat and momentum transfer in laminar flow with helium initially at extremely high temperature (3,000 - 15,000°R). The heat exchanger was composed of three copper units each approximately 1 inch long, 0.125 inch I.D. and water-cooled. It was found that the heat transfer rates from the gas were as high as 2,500,000 BTU/hr.ft^2 and average heat transfer coefficients of 310 BTU/hr.ft^{2}F.

Small-sized and water-cooled heat exchangers were usually employed by the above researchers in the various studies. The plasma jet was actually in contact with the walls of the heat exchanger. The local heat transfer coefficients and heat transfer rates accordingly would be quite high. However, with a larger heat exchanger, enclosing the hot gas emerging from the plasma jet, heat transfer characteristics will be different as shown in the second part of this report.

3. EXPERIMENTAL APPARATUS

The assembly of the test apparatus is shown in Figure 1. Essentially the test equipment consisted of three parts, namely the d.c. power source, the plasma generator and the heat exchanger. The high current was fed to the plasma generator to sustain the plasma arc. The plasma jet formed then became the heat source for the heat exchanger. The performance characteristics of the plasma generator and the heat transfer phenomena from the high temperature gas to the cold wall were studied.

3.1 The Power Source

The power supply circuit is shown in Figure 2. The line source was fed into the Superior Electric Powerstat*. The powerstat provided the primary control of the volt-ampere supply to the plasma arc. The transformer and the rectifier for conversion of a.c. power to d.c. power were purchased as a combined unit - the Powertronic Rectifier** supplying 110 volt and 91 ampere direct current. The power supply was also used as a d.c. power source for other experiments in the Mechanical Engineering laboratory. In addition to the powerstat control, a slide-wire type resistance was connected in

*The Superior Electric Powerstat, model 1256C-1400 - Input 575 V. 3Ø60 cps. Output 0-575 V. 28 amps.

**The Powertronic Rectifier Type 260R - Input 575 V. 14.6 amp. 3Ø60 cps. Output 110 d.c. V. 91 amp.

series with the arc circuit to provide further adjustment on the potential gradient across the arc.

The arc potential and current were measured with appropriate electrical meters* mounted on the instrument panel (see Figure 1).

3.2 The Plasma Generator

The mechanical design of the plasma generator was undertaken by D. Male as his design project in Mechanical Engineering, 1961-62, at McMaster University. Preliminary experiments on the original plasma generator revealed some undesirable operating characteristics. Minor changes were carried out by the author to eliminate leakage along the gas path, to reduce the possibility of arcing between the anode and its holder, and redesign of the cathode holder to permit water cooling. The final design of the plasma generator is shown in Figure 3.

The plasma generator consisted of a NC50 graphite porous electrode**, which was firmly positioned in the water-cooled brass holder, by a water-cooled copper pressure plug. The firm contact between the pressure plug and the electrode was maintained by a compression spring*** placed inside the micarta insulation socket. Flexible braided copper connectors bypassed the insulation socket and completed the electrical circuit to the power supply.

The porous-electrode holder was positioned at the front of

*Simpson d.c. voltmeter - model 1329SC - 0.50 V. Simpson d.c. millvoltmeter - model 1329SC - 0-100 divisions (100 amp. shunt model 766).

**Ordered from National Carbon Company, Cleveland, Ohio, U.S.A.

***Designed to order by R. Hick, 1962-63, fourth-year Mechanical Engineering student, McMaster University. Ordered from Hi-Bek Precision Spring Co., Hamilton.

a cylindrical brass body by eight screws, while the assembly of the water-cooled pressure plug, the cooling water inlets and outlets for the pressure plug, the insulation socket, etc., was placed inside the brass body and compressed against the porous electrode by a combination brass-micarta retaining plate at the back of the brass body. A second set of eight screws was used to hold the retaining plate in position. The cooling water inlets and outlets for the porous-electrode holder were connected to the back of the brass body through eight Swagelok fittings.

A thin asbestos paper coated with a layer of "Sauereisen"* insulated the porous electrode from its holder. A suitable O-ring around the pressure plug acted as a seal to the back-flow of the gas and also as additional electrical insulator. Arcing between the sides of porous electrode and its holder was then successfully prevented.

The brass body containing the porous electrode was seated inside a micarta insulation casing to the front of which the other electrode holder could be attached. It can be seen from Figure 3 that the brass body could be adjusted to travel linearly inside the insulation casing, thus permitting the operator to vary the electrode gap distance while the generator was in operation.

The second electrode took the form of a water-cooled copper spool having a central hole of 0.625 inch diameter. Thus the emerging jet had a maximum diameter of 0.625 inches. The electrode was then embedded in a brass plate 0.5 inches thick. This plate was

*Trade name for insa-lute adhesive cement No. 1 paste, Sauereisen Cements Co., Pittsburgh, Pennsylvania, U. S. A.

recessed to position the electrode centrally and also drilled to provide cooling water to enter and exit from the spool. A single splitter plate produced a circulatory flow path around the spool.

Argon was used as the transpiration fluid throughout the experiment and supplied from the ordinary gas cylinder. The gas flow and the gas exit pressure were controlled by a Harris multi-stage regulator* and metered through a Dry-Test type gas meter**. The gas flow rate was found with the aid of a stop watch.

A high voltage starter was used to initiate the plasma arc. Its function was essentially to cause local ionization of some of the neutral gas atoms around the starter. Once the ionization had reached a certain level, the plasma arc was formed and sustained by the external electric field.

Due to the brightness of the plasma arc, which was roughly equivalent to direct sunlight, No. 10 welding lenses*** were worn during the experimental runs. For demonstration purposes, the plasma jet was completely enclosed in a 5.50 inch diameter pyrex tube covered by two or three layers of deep colored "cellophane" paper.

Cooling water for the electrode holders was supplied directly from the floor mains in the building. Plastic hose was used for the water passages and insulated with fibreglass wool where necessary. Clear plastic pockets were used as thermometer holders at the inlets and outlets of the flow passages. The plastic pockets were designed

* Harris multi-stage regulator type 92-200.
** American dry test meter type AS-11-5-25B, W.P. 100 psi.
*** Welding filter lenses manufactured by the Welsh Manufacturing Co., Providence, R.I., U.S.A.

to provide a proper immersion depth (3.0 inches) of the thermometer and also good mixing at the thermometer bulb. The presence of air bubbles could also be shown. Suitable O-rings were used as water and gas seals in all major connections.

3.3 Heat Transfer Equipment

Figure 4 provides an isometric view of the heat transfer test section. The test section is essentially a double-walled single-pass parallel-cocurrent flow heat exchanger, the inside tube of which was a thin-walled stainless steel tube having an outer diameter of 1.500 inches and a wall thickness of 0.035 inches. One end of the tube was welded to the water inlet assembly (see Figure 4). The other end of the thin-walled tube extended beyond the overall length of the heat exchanger and was closed with a filter lense fitted in a window through which the action of the plasma jet could be observed. Just prior to the downstream end, the tube was opened to two outlets at 180° apart, one for the exhaust of the gas and the other included for further instrumentation. On opposite sides of the outer wall of the stainless steel tube the thermocouple locations were marked and milled to 0.010 inch deep with a thin circular saw. When the thermocouples were being installed, the electrically welded hot junctions were embedded in the grooves to give more accurate wall temperature measurements.

The outer casing of the heat exchanger was a thick-walled brass tube with an I.D. of 2.375 inches, split into two halves. Along the split surface, a long semi-circular groove with a radius of

0.125 inches was machined. This permitted a rubber O-ring strip to be installed as a water seal during assembly.

In order to test for the symmetry of the plasma jet, the annular cross-section of the double-walled heat exchanger was divided into four equal parts as shown in Figure 4. The dividers were made up of four 0.125 inch x 0.625 inch longitudinal strips of teflon, equally spaced inside the brass split tube, making an angle of 45° with the horizontal plane. These teflon strips were designed to rest on the inner tube and to provide water-tight joints between the flow passages under the compression pressure of the external steel clamps. This would permit equal flow rates of the cooling water through the four parts of the annulus. The shape of the cross-section also provided better mixing of the cooling water.

On each half of the brass tube, twelve Swagelck fittings* at specified intervals permitted the installation of the bulk temperature probes (see Figures 4 and 5a). Outlets were also provided for the thermocouple leads fastened to the wall surface of the inner tube. Each outlet was located beside the Swagelok fitting described above, and consisted of a short piece of hypodermic tubing positioned by a modified capscrew resting against a small O-ring. The opening in the hypodermic tubing between the wires was later sealed with silicon rubber cement**.

A semi-circular brass plate was silver-soldered to the ends

*Swagelck fitting - Part No. 200-1-2, 1/8" tube to 1/8" pipe with teflon ferrules.

**General Electric Silicone Products, type RTV-102, New York, U.S.A.

of each half of the split tube for fastening, and rubber O-rings were again used to seal against coolant leaks. On assembly with the thermocouples and teflon separators in place, the inner tube was lowered to rest on the bottom half of the split tube.. The thermocouple wires were carefully let out through the corresponding outlets. The rubber O-ring strips were laid in the milled grooves on the split surface. Some liquid silicon rubber was smeared evenly on the O-ring strips to ensure better sealing. The top half of the split tube was then lowered to the inner tube and the thermocouple wires were again carefully let out through the corresponding openings. With the long O-ring strip properly in place, both ends of the outer tube were fastened to the inner tube assembly. Four heavy steel clamps were used to hold the O-ring strips and the teflon separators in the correct resting position.

Fibreglass wool (approximately 0.5 inches thick) wrapped along the heat exchanger was to insulate the outer wall of the heat exchanger against possible room temperature effects.

The whole assembly rested on two steel cradles which were fastened to the test table as shown in Figure 1.

3.4 Experimental Instrumentation

Since the study of the performance characteristics of the plasma generator and the heat transfer phenomena is based on the measurement of the power input, the gas flow, the cooling water rates, and various temperatures, a description of the necessary instrumentation is required here.

The cooling water-rate of the anode holder was measured downstream by means of a Reynolds column which consisted of a 2 inch I.D. brass pipe with an orifice plug screwed into the threaded bottom of the cylindrical reservoir. The head of the water column was registered by a gauge glass tube connected to the reservoir 2 inches above the orifice plane. After leaving the water jacket the cooling water entered the reservoir and was discharged at atmospheric pressure. With proper design of the orifice opening, The Reynolds column could be made to handle the cooling water flow rate over the required range. For the present purpose, the orifice opening had a diameter of 0.1563 inches, measuring a flow rate up to 4.50 lbm/min. with a head of 30 inches of water.

The Reynolds columns were all calibrated using weighing tanks under normal operating conditions. Since the density of water is practically a constant in this temperature range a dingle calibration curve is all that is required. The calibration curve is shown in Figure 19.

The cooling water flow rate of the cathode holder was measured with a calibrated measuring tank. A total flow of 3, 4 and 5 gallons was each timed with a stop watch. An average flow rate of the cooling water was taken during the test run.

The argon fluid flowwas supplied from the commercial bottles and regulated with a Harris multi-stage pressure regulator and measured by an American Dry Test Meter. The gas flow rate at a certain exit pressure in the gas bottle was determined by registration of the total flow on the gas moter per unit time. The calibration procedure was repeated at different gauge pressures to obtain a mean calibration curve (see Figure 20). With the same flow resistance in the path of the gas flow, the gauge pressure could then be used to indicate the gas flow rate directly.

To measure the inlet and outlet temperatures of the cooling water for the plasma generator and the heat transfer equipment, mercury-in-glass precision thermometers* were used with the range of 35°F to 75°F and installed in the thermometer pockets designed to provide the correct immersion depth.

The Simpson meters were used to measure the potential gradient across the plasma arc and the current through it. Due to the oscillatory action of the arc, only the average values were recorded for data computations.

For the study of the heat transfer characteristics from the high temperature gas along the double-walled heat exchanger, the wall temperatures of the stainless steel tube and the bulk temperatures of the cooling water in the annulus were measured by means of copper-constantan thermocouples, located at twelve stations diametrically opposite to each other. Figure 4 shows the arrangement, the spacings of the thermocouples, and the details of the thermocouple installation.

Each thermocouple assembly measuring the water bulk temperature consisted of eight feet of Thermo Electric TG-26-DT copper-constantan thermocouple wire with one end potted inside a 0.125 inch x 2.5 inch

*Casella London Thermometers - type mercury-in-glass, solid stem with National Physical Laboratory (England) Certificate guaranteeing an accuracy of ± 0.01°F.

protection tube. The hot junction was exposed 0.25 inches from the end of the tube whose final length of 0.5 inches was bent 90° (see Detail 1, Figure 4).

At the same station, the hot junction of the Thermo Electric TG-30-DT copper-constantan thermocouple wire was embedded inside the milled groove in the wall of the stainless steel tube, 0.010 inches below the cool surface. The wall temperature on the gas side was estimated by calculating the temperature drop across the tube wall as shown in Appendix D.

The thermocouples, 24 bulk and 24 surface, were terminated in a Thermo Electric 48 circuit jack panel*. A Philips millivolt recorder** was used to measure the thermo electric power of the thermocouples.

Twelve Thermo Electric 2PSS type copper-constantan plugs connected the recorder to the jack panel and enabled the thermoelectric power of any twelve thermocouples to be recorded at the same time. The millivolt readings were then converted to temperatures with a standard conversion table*** for copper-constantan thermocouples.

To further the investigation of the heat transfer characteristics from the hot gas leaving the plasma arc, a temperature probe

*Thermo Electric jack panel - bakelite, copper-constantan calibration and individually numbered.

**Philips millivolt recorder - model PR3210 A/00 12-point self-balancing.

***Prepared by General Electric Co., based on the International Temperature Scale of 1945.

(see Figure 5b) was constructed in the form of a hollow tube, five feet in length and an outside diameter of 0.125 inches. Four spider-supports with spacing feet at 120° apart were welded to the small tube and held the probe body in a central position with respect to the stainless steel tube. A Ceramo chromel-alumel thermocouple* was then fed through the tube and held in position with set screws. The hot junction protruded approximately 4 inches from the first spider support. The probe allowed the measurement of the bulk temperature variation of the hot gas along the tube. Twenty-six locations were marked on the probe. The probe was then adjusted by hand to travel inside the tube. (At that time the view lense at the rear end of the heat exchanger was already removed.) A Rubicon precision potentiometer** was used to measure the millivolt output of the thermocouple against the ice point.

Temperatures were obtained with the probe to within approximately 0.5 inches from the plasma jet. At a closer distance, the hot junction of the thermocouple melted and fused with the outside casing.

As a further and more accurate check on the bulk temperature rise from station to station, the jack panel enabled the bucking of any two outputs. The bucking of two thermocouples was accomplished by using two Thermo Electric 2PSS type copper-constantan plugs, with the constantan ends short-circuited and the copper ends connected to precision potentiometer. The plugs could then be connected to the jack panel at two points whose temperature difference was to be

*Thermo Electric thermocouple wire, type CES 10-116-CT.

**Minneapolis-Honeywell Reg. Co., Rubicon Instrument Model No. 2745, U.S.A.

measured.

The Rubicon precision potentiometer was also employed to spot-check the water bulk temperatures across the annulus to ensure that the true bulk temperature was being measured at each station.

All direct thermocouple measurements were referenced to the ice point.

4. EXPERIMENTAL PROCEDURE

The experiment consisted of two main parts namely the study of the plasma generator characteristics and the study of heat transfer phenomena from a high temperature gas stream. For the bulk of the experiments concerning both the generator characteristics and the heat transfer phenomena, the electrode spacing and the argon gas flow rate were held constant. In this section, the experimental procedure for each part will be described in order.

4.1 The Study of the Plasma Generator Characteristics

The study of the plasma generator characteristics was performed in the following order.

4.1.1 General Characteristics

Following the work of Sheer (9), preliminary experiments were performed to test for the erosion rates of the cathode materials and the arc stability. The cathode materials included inconel and several grades of carbon, namely type AUC, ATJ and commercial*. The same design of cathode was constructed for each case having a central hole of 0.5 inch diameter, and a thickness of 0.125 inches.

Other transpiration fluids, namely nitrogen, oxygen and dry

*Supplied by National Carbon Company, Cleveland, Ohio, U. S. A.

air at various flow rates were also used to test for arc stability.

As a result of the above tests the plasma generator was redesigned using a water-cooled copper anode and a transpiration-cooled porous cathode. Arc stability and low erosion rate of the cathode were observed, permitting long runs to be carried out. The modified plasma generator was then employed in the study of the other characteristics as described in later paragraphs.

4.1.2 The Influence of the Transpiration Fluid Flow on the Arc Voltage

The study was made at a constant arc current of 70 amperes. By adjusting the Harris-multi-stage pressure regulator, different flow rates of argon were obtained. For each particular gas flow, the corresponding arc voltage was recorded. The arc current was maintained constant by adjusting the powerstat connected to the power supply.

4.1.3 The Voltage-Current Characteristics

The gas flow and the electrode gap distance were held constant. When the temperatures of the cooling water were stabilized, the gas flow and the power were turned on, supplying a gas flow of 2.50 cu.ft./min. and an electric potential of 110 d.c. volts across the gap. A high voltage starter was employed to start the arc, and once the plasma arc was initiated the voltmeter was then connected across the arc gap to measure the potential drop.

The voltage-ampere variations were obtained by controlling the slide-wire resistance connected in series with the plasma arc and the powerstat connected to the primary side of the power source.

4.1.4 The Cathode Erosion Rate

The NC50 graphite porous plug cathode was carefully weighed using a Mettler balance* before and after each experimental run as described in paragraph 4.1.3. An average erosion rate of the cathode was obtained at different power inputs and with the constant gas flow rate.

4.1.5 The Efficiency of the Plasma Generator

When constant flow rates of the cooling water and stabilized water temperatures were obtained, a gas flow rate of 2.50 cu.ft./min. was supplied and the arc initiated.

The plasma arc was maintained until the necessary measurements under steady-state conditions had been acquired. The measurements included the arc voltage, the arc current, the gas flow rate, the cooling water rates for the anode holder and for the cathode holder, the inlet and outlet temperatures of the cooling water, the room temperature, and the time of run.

The same procedure was performed at different power inputs.

4.2 Heat Transfer Measurements from the High Temperature Gas Flow

The cooling water for the double-walled heat exchanger was supplied from the water-mains in the building. Prolonged running of the cooling water was necessary to establish the constant flow rates and stabilized water temperatures.

*Mettler balance, type H5, model No. 54345.

The flow-rate of the cooling water leaving each longitudinal section of the heat exchanger was measured with a Reynolds Column. The water flow-rate in each section could be adjusted by applying back pressure at the exit plane by means of a hose clamp.

The cold junctions of the thermocouples were immersed in an ice-bath and the thermocouple recorder turned on. When steady milli-volt readings were recorded on the recorder and equal flow rates of the cooling water were registered for all four sections, the plasma arc was then started with the required gas flow rate and power input adjusted.

For these tests, the plasma generator body was removed from the pipe stand (Figure 1) and mounted on a traversing device, This device permitted not only the horizontal but also the vertical alignment between the plasma generator body and the front end of the heat exchanger. Once this alignment had been obtained, the generator body could be moved away from the heat exchanger and the arc initiated. The generator body then carrying the plasma jet was moved back into position. Two vise grips were used to hold the anode disk of the plasma generator flush against the circular front end of the heat exchanger, with a circular mica ring* between them acting as an insulator and a gasket. In this way, the leakage of the ambient air into the hot argon jet was prevented.

When steady state conditions were reached after 15 - 20 minutes of running time, the necessary measurements were taken. All

*India Moulding Plate, No. 1-1011, H. P. Ruggles Co. Ltd., Hamilton the wall and bulk temperatures as measured by the copper-constantan thermocouples were recorded by making proper connections between the twelve copper-constantan plugs, and the 48 circuit jack panel. The other measurements included the inlet and outlet temperatures of the cooling water and the water flow rate for each section, the gas flow rate, the gas outlet temperature, the room temperature, the voltmeter and ammeter readings, and the electrode gap distance.

In order to provide a check in the bulk temperature rise of the cooling water between any two successive stations, a separate measuring system enabled the bucking of any two thermocouples, the emf difference being read by a Rubicon precision potentiometer. Spot-checks were also made on the bulk temperature variations at some stations to ensure that measurements taken were representative of the true bulk temperatures.

The hot gas temperatures along the axis of the inner tube were then measured at 26 locations, using the chromel-alumel temperature probe. The probe was unshielded, as the cross-section of the thermocouple tip was to be kept as small as possible. However, necessary corrections were made to account for the radiation effects.

Further heat transfer measurements were carried out with variations in the cooling water flow rates while the power input and the gas flow rate were maintained constant.

5. ANALYSIS OF THE EXPERIMENTAL RESULTS

The experimental and calculated results are tabulated under the appropriate headings in Appendix A. The data evaluations and error analysis will be described in the following paragraphs.

5.1 Data Evaluations

The power input of the plasma arc was calculated by

$$P = V\ I \text{ watts} \tag{1}$$

The efficiency of the plasma generator can be defined as the ratio of the measured enthalpy to the theoretical enthalpy of the effluent plasma jet. The measured enthalpy corresponds to the energy absorbed by the gas passing through the plasma arc, and the theoretical enthalpy is the arc power input. The efficiency of the plasma generator was then estimated by considering the energy losses to the cooling water for the electrodes. The energy loss to the anode cooling water was calculated by the following relation,

$$Q_{wa} = m_{wa}\, C_{pw}\, (t_2 - t_1) \tag{2}$$

while the energy loss to the cathode cooling water was given by

$$Q_{wc} = m_{wc}\, C_{pw}\, (t_3 - t_1) \tag{2a}$$

The radiation loss at the copper anode was negligibly small as approximated by the relation, (see Appendix B)

$$Q_{ra} = \varepsilon_c \sigma T_a^{\,4} A_a \tag{3}$$

The efficiency of the plasma generator was found by the relation

$$\eta = 1 - \frac{Q_{wa}+Q_{wc}}{P}$$

As a matter of interest the heat transfer rate at the water-cooled anode could also be evaluated by $(Q/A)_a$ where $A = \pi d_a \ell$, the heat transfer area of the anode.

For a certain gas flow and power input, the temperature of the plasma arc could be calculated based on the average efficiency of the plasma generator and also with the aid of Saha's equation relating the degree of ionization to the equilibrium temperature. The necessary assumptions for the use of the above method will be discussed in Section 6. In this method, the rate of ionization was determined from the available arc energy and the ionization potential of the argon atom. The amount of neutral atoms present can be derived from the gas flow rate. Then the degree of ionization, ϕ, could be interpreted as the ratio of the number of ionized particles to the number of neutral atoms present; that is

$$\phi = \frac{\eta P/u_I}{M_g N} \qquad (4)$$

where η = the efficiency of the plasma generator

P = the arc power input, joules/sec.

u_I = the first level ionization potential of argon, joules/ion

M_g = gas flow rate, kg.-mole/sec.

N = Avogadro's number, particles/kg-mole

The temperature of the plasma arc was then obtained from the simplified Saha equation (24) which follows,

$$\frac{\phi^2}{1-\phi^2} p = 3.16 \times 10^{-7} T_E^{5/2} e^{-u_I/kT_E} \quad (5)$$

where ϕ = the degree of ionization

p = the ambient pressure of the plasma arc, atm.

T_E = the equilibrium temperature, ^oK

u_I = the first level ionization potential of argon, joules/ion

k = the Boltzmann constant, 1.38×10^{-23} joules/^{o}k

The equation is plotted in Figure 13 with ϕ as a function of T_E.

The temperature measurements made in the experiment allowed studies to be made on the local heat transfer coefficients and the heat transfer rates from the hot gas to the cooling water in the annulus. Firstly, the measurements made of the gas temperatures were considered. These readings as obtained from the movable chromel-alumel thermocouple were corrected for radiation losses from the hot junction to the cold wall by taking a heat balance at the junction. The heat balance can be written as follows:

$$q/A_t = h_{gt} (T - T_t)_x = \varepsilon_t \sigma (T_t^4 - T_s^4)_x \quad (6)$$

The average heat transfer coefficient $\bar{h}_{gt}$ was estimated by considering that the thermocouple junction was spherical in shape and the heat transfer process at the junction was by forced convection. The relation used was given in Reference 25 as the following,

$$\frac{\bar{h}_{gt} d_t}{k_{gc}} = 0.615 \left(\frac{m_g . D_e}{A_c \mu_{gc}}\right)^{0.466} \quad (7)$$

In equation 6, an average value of the wall temperatures was used, since at each station two diametrically opposite readings were available. This practice did not introduce any noticeable error as the gas-to-wall temperature difference was quite high. The temperature drop across the thin wall of the stainless steel tube was found to be fairly small (see Appendix D), and accordingly the wall temperatures were applied without corrections.

One of the major difficulties in the calculations for the heat transfer coefficients and other quantities was due to the changes of the physical properties of the gas as a function of temperature. The gas inlet temperature in the heat exchanger was measured with the adjustable probe up to approximately 3000°R. The exhaust temperatures for all tests were around 800°R. A large axial temperature gradient was therefore expected. As the average wall temperature was about 530°R, a large radial temperature gradient could also be expected in the gas flow. The physical properties of argon as a function of temperature were obtained from the report by Hilsenrath and Touloukian (26) which provided the required information for temperatures up to about 2700°R. Values at higher temperatures were found by extrapolation, and checked with the formulae provided in the report.

The corrected gas temperatures, the water bulk temperatures and the wall temperatures were plotted as a function of the distance along the tube. The method of the least mean squares was used to find the best fitting curves through the experimental points. For the following computations on heat transfer, the temperatures were read directly from the best fitting curves.

Sufficient information was then available to calculate the energy lost by the hot gas and the energy gained by the cooling water.

The calculation was carried out with the aid of two expressions. The first one describes the heat balance of the hot gas at each marked station along the tube, as given in the usual manner by $m_g C_{pg}\left[T_{x+\Delta x} - T_x\right]$. The second expression corresponded to the heat balance of the cooling water at the same station, defined by $m_w C_{pw}\left[t_{x+\Delta x} - t_x\right]$. When some differences were found between the values of the energy transfer, the gas bulk temperatures were calculated by the following relation based on the energy balance of the cooling water,

$$-\left[T_{x+\Delta x} - T_x\right]_{\text{calculated}} = \frac{m_w C_{pw}\left[t_{x+\Delta x} - t_x\right]}{m_g C_{pg}} \qquad (8)$$

The calculated gas temperatures and the measured gas temperatures were compared. Then, the local heat transfer coefficients on the gas side, h_{gs}, were separately calculated by equations (9), (10), as follows:

$$h_{gs} = \frac{-m_g C_{pg}\left[T_{x+\Delta x} - T_x\right]}{A_i\left[T_{gc} - T_{ss}\right]_{\text{measured}}} \qquad (9)$$

$$h_{gs} = \frac{m_w C_{pw}\left[t_{x+\Delta x} - t_x\right]}{A_i\left[T_{gb} - T_{ss}\right]_{\text{calculated}}} \qquad (10)$$

The resulting limits of h_{gs} should provide a close estimation of the range in which the true h_{gs} would fall.

The dimensionless parameters to be computed at each station (26 stations altogether) along the tube included the Nusselt number, $h_{gs}D/k_g$, the Reynolds number, $m_g D/A_c \mu_g$, the Grashof number, $g\beta\Delta T D^3/\nu_g^2$, the gas-to-wall temperature ratio T_{gb}/T_{ss}, the length-to-diameter ratio x/D and the non-dimensional tube length $x/D/Re_x Pr$. The dimensionless parameters were calculated only at the local mean film temperature, $T_{gf} = ½\left[T_{gb} + T_{ss}\right]$. The characteristic length in the computation of the dimensionless parameter was the inside diameter of the inner tube.

The tabulated results given in Appendix A are also presented in graphical form, so that they can be more easily interpreted. For the performance characteristics of the plasma generator, the graphical presentation includes, (i) the effect of the transpiration fluid flow on the arc voltage at constant current (Figure 9), (ii) the voltage-ampere relation at constant gas flow rate (Figure 10), (iii) the cathode erosion rate as a function of the power input (Figure 11), (iv) the efficiency of the plasma generator as a function of the power input at constant gas flow rate (Figure 12) and (v) the estimation of the arc temperature as a function of power input (Figure 14).

The bulk temperatures of the hot gas, the wall temperatures, the bulk temperatures of the cooling water, and the gas-to-wall temperature ratios are plotted as a function of the axial distance along the tube in Figures 16a and 16b. In Figure 17, the variations of the local heat transfer coefficients along the tube are shown. Finally the local Nusselt numbers are plotted in Figure 18 as a function of the non-dimensional tube lengths, $x/D/Re_x Pr$, with the dimensionless parameters evaluated at the film temperatures on the gas side.

5.2 Error Analysis

In this section, the uncertainties in the measurement of the experimental data and the calculated results are presented in a tabulated form. Due to the oscillatory nature of the arc process, the plasma jet also exhibited a random fluctuation. This fluctuation was not of high amplitude, but it could be observed in the measurement of the arc voltage and current, and also was evident in the measurement of the gas temperatures. The effect of the jet fluctuation was less noticeable and of course was dampened as the gas and the cooling water flow progressed down the heat exchanger length.

The specific heat of argon taken from Reference 8 and the fluid properties of the cooling water from Reference 30 were assumed constant without introducing any appreciable error.

The method of estimating the error in the data computations was based on Reference 32. For example the maximum absolute error modulus in a sum (difference) is equal to the sum of the absolute error moduli of the separate terms. The maximum relative error in a quotient or a product is equal to the sum of the relative errors in the various factors.

Description	Symbol	Instrumental Error	Experimental Error	Maximum Error
Arc voltage	V	Negligible	± 5% - due to the fluctuations of the voltmeter readings	± 5%
Arc current	I	Negligible	± 2% - due to the fluctuations of the ammeter readings	± 2%
Gas Flow Rate	m_g	± 2% - based on the calibration curve	Negligible	± 2%
Water Flow Rate	m_w	± 3% - based on the calibration curve	± 1% - due to slight fluctuations of the water level	± 4%
Temperature (measured by precision thermometers)	t	± 5% (.1°F) - guaranteed accuracy by manufacturer	Negligible	± 5%
Temperature (measured by cu-const. thermocouples)	t_x T_{ss}	Negligible	± 5% - based on the best-fitting curve	± 5%
Temperature (measured by Cr-Aℓ thermocouple)	T_x	3/4% - guaranteed accuracy by manufacturer	± 5% - based on the best-fitting curve	± 5 3/4%
Thermal conductivity	k_g	± 3% - based on Hilsenrath and Touloukian (26)		± 3%
Viscosity	ν_g, μ_g	± 2% - based on Hilsenrath and Touloukian (26)		± 2%

Description	Symbol	Relation	Maximum Uncertainty
Arc power input	P	$P = VI$	$\pm$ 7%
Energy losses to electrodes	Q_{wa}	$Q = m\, C_{pw}\, \Delta t$	$\pm$ 6%
Efficiency of plasma generator	η	$\eta = 1 - \frac{Q_{wa} + Q_{wc}}{P}$	$\pm$ 15.6%
Degree of ionization	ϕ	$\phi = \frac{\eta P}{u_I} / M_g N$	$\pm$ 17.6%
Maximum arc temperature	T_E	$\frac{\phi^2}{1-\phi^2}\, p = 3.16 \times 10^{-7}\, T_E^{\frac{5}{2}}\, e^{-\frac{u_I}{kT_E}}$	$\pm$ 14.0%
Energy balance of cooling water	q_w	$q_w = m_w C_{pw} \Delta t_x$	$\pm$ 14.0%
Energy balance of hot gas	q_g	$q_g = m_g C_{pg} \Delta T_x$	$\pm$ 12.0%
Local heat transfer coefficient (i) based on energy balance of cooling water	h_{gs}	$h_{gs} = \frac{m_w C_{pw} \Delta t_x}{A_i (T_{gb} - T_{ss})}$	$\pm$ 36.0%
(ii) based on energy balance of hot gas	h_{gs}	$h_{gs} = \frac{m_g C_{pg} \Delta T_x}{A_i (T_{gc} - T_{ss})}$	$\pm$ 35.0%
Local Nusselt number	Nu_x	$Nu_x = \frac{h_{gs} D}{k_{gf}}$	$\pm$ 36.0%
Local Reynolds number	Re_x	$Re_x = \frac{m_g D}{A_c \mu_{gf}}$	$\pm$ 4.0%
Local Grashof number	Gr_x	$Gr_x = \frac{g \beta \Delta T D^3}{\nu_{gf}^2}$	$\pm$ 19.0%
Non-dimensional tube length	$\frac{x/D}{Re_x Pr}$	-	$\pm$ 4.0%

6. DISCUSSION OF RESULTS

6.1 The Performance Characteristics of the Plasma Generator

In this section, the characteristics of the plasma generator based on the original design and the modified will be discussed in order.

6.1.1 General Characteristics

All the early studies were made with the original plasma generator having "forward-polarity", that is the porous graphite plug through which the transpiration fluid emerged as the plasma jet was the anode and the downstream carbon disk was the ring cathode. Several cathode materials, namely type AUC, ATJ and the commercial carbon, were used to test for arc stability and erosion rate.

Figure 7 shows the picture of three eroded cathode disks of different grades of carbon. During each run, the cathode spot was observed to oscillate slowly between two points approximately 120° apart. After 15 - 20 minutes of each run, the cathode spot tended to stay at one of the two points and erosion continued resulting in a skewed jet. When the gas flow was increased, a twin-jet was obtained with the cathode jet parallel and attached to the plasma jet (the main column) and the arc became highly unstable, as indicated by the large fluctuations in the arc voltage and current readings. At a higher gas flow rate, the arc was blown out and the experiment interrupted.

Generally speaking, the degree of assymetry of the plasma jet and the erosion rate of the cathode varied with the gas flow rate, the cathode material and the power input. These conditions were considered undesirable for prolonged operation of the plasma generator, especially in the related heat transfer studies.

In Figure 8, the example of an inconel "cold cathode" is shown. The term "cold cathode" refers to metal cathodes which do not have the property of "thermionic emission" even at high temperatures, up to the melting point of the metal. The usual phenomena accompanying the "cold cathode" were noted, for example the existence of several cathode spots at the same time, the irregular motion of the cathode spot, and the melting of the cathode material. Similar features were present when a water-cooled copper cathode was used.

While the erosion rate of the cathode was considerably fast, the porous anode plug remained intact, largely due to the cooling effect of the transpiration fluid.

Due to the fast erosion rate of the cathode and a skewed jet obtained at high gas flow rates, the original design of the plasma generator was modified. A water-cooled copper electrode was introduced and replaced the carbon ring cathode. The polarity was reversed, so that the former porous graphite plug became the cathode and the water-cooled copper spool the anode. A steady arc process was achieved at high gas flow rates and the jet remained symmetrical. The anode which was cooled by fast-running water retained its original circular shape all through the experimental runs.

Pictures of the plasma jet in operation are shown in Figure 6.

The size of the jet was visually estimated to be approximately 1.50 - 2.0 inches long and 0.625 inch in diameter. The jet size, in general, varied with the gas flow, the power input and the electrode gap distance.

When other transpiration fluids, such as nitrogen, oxygen and dry air, were used, the electric arc was highly unstable. In other words, the arc, once started at a very small electrode gap distance, could not be sustained by the external field. Explanation of this situation would involve further study in spark breakdown process, the description of which is beyond the scope of this report. However, one logical way to provide a simple explanation is to realize that the other fluids are diatomic. In general, diatomic gases would have to be dissociated first before ionization can take place. This process of dissociation requires a certain amount of energy (the dissociation potential) in addition to the ionization potentials of the products of dissociation. For example, the dissociation potentials for nitrogen and oxygen are 9.1 and 5.1 volts respectively. For argon, of course, it is zero. Furthermore, the spark-breakdown voltages for argon, nitrogen, air and oxygen are given (31) respectively as 137, 251, 327 and 450 volts. A comparison of the dissociation potentials and the break-down voltages between argon and other diatomic fluids may serve to explain why argon was used all through the experiment.

It may be worth mentioning that, if the electrodes are made of carbon, nitrogen should be used with extreme care. At the plasma arc temperature, some poisonous carbon-nitrogen compounds may be easily formed.

6.1.2 The Effect of Gas Flow Rate on Arc Voltage

The influence of the gas (argon) flow rate on the arc voltage at constant arc current and electrode spacing is shown in Figure 9. The general trend of the curve agrees closely with that obtained by Sheer (9) who worked with a transpiration-cooled anode. The transition from an unstable mode of arc operation to a relatively stable mode was observed using the modified electrode configuration, i.e., with reversed polarity. The transition was also accompanied by a sudden rise in the arc voltage and ended at a gas flow rate of approximately 122 gm./min. Although a water-cooled copper anode was used, the similar steady arc operation beyond the gas flow of 122 gm./min. reveals that the high intensity arc mode was achieved. Moreover, a further increase in the gas flow rate did not seem to cause any instability. The fact that the porous plug was being used as the cathode eliminated the blow-out of the cathode jet and permitted the test to be continued at a high gas flow rate.

6.1.3 The Voltage - Current Relation

Figure 10 shows the voltage-current relation at a constant gas flow of 122 gm./min. Although there is some scattering of the experimental points the positive slope of the curve indicates the steady arc operation with the gas flow acting as a d.c. resistance (9). As mentioned in the previous paragraph, the increase of gas flow would increase the arc voltage at constant current. Accordingly, it may be expected that the increase of gas flow tends to increase the d.c. resistance of the discharge. On the other hand, the linear relationship of the Ohm's Law given in the elementary form ($V = IR$) will not hold with respect to the terminal voltage, current and the gas flow acting similarly to a d.c. resistance.

6.1.4 Cathode Erosion

The average cathode erosion rate has been found to be approximately 0.011 gm./min. The relatively low erosion rate of the cathode is largely attributed to the cooling effect of the transpiration fluid. Under normal operations, the cathode plug with 0.5 inch in diameter and 0.125 inch neck lasted for more than 90 minutes without causing any instability of the jet. The duration was considered satisfactory for the present purpose. The cathode erosion rate is shown in Figure 11a and an example of an eroded cathode plug can be seen in Figure 11b.

6.1.5 Efficiency of the plasma Generator

The efficiency of a plasma generator describes the amount of the arc power that can be transferred to the gas enthalpy. In this experiment, the average efficiency was found to be 59%.

The average enthalpy of the emerging plasma jet as measured later by the cooling water in the double-walled heat exchanger amounts to roughly 61% of the arc power. However, this appears low, as the gas exit temperature was actually higher than the room temperature. If the gas enthalpy was calculated by $H = m_g C_{pg} \Delta T$, where ΔT was the temperature difference between the exit gas temperature (room temperature) and the temperature of the gas leaving the plasma jet, the gas enthalpy would be approximately 64% of the arc power.

These values of the efficiency compared favourably with those obtained by considering just the arc energy losses to the electrodes. C. Sheer (9), F. Schoeck and E. Eckert (8) reported an efficiency up to 87 - 88% with the transpiration fluid-cooled anode, while Knipe, Stokes and Streng (21) reported an efficiency of 56% with the water-cooled copper anode.

The discrepancy between the two configurations can be explained by the fact that the gas increases its enthalpy when flowing through the anode fall space and absorbing a large amount of the kinetic energy and the energy of condensation of the electrons. Furthermore, the kinetic energy of the electrons in the anode fall space increases in high intensity arc operation as the potential drop across the fall space is relatively large. In the present experiment, the gas flow was in the same direction as the electron drift velocity and the gas may not all pass through the anode fall space. In this way, most of the energy in the anode fall space was carried away by the anode cooling water, instead of being used to heat up the effluent gas stream. Accordingly, the energy transfer efficiency obtained in the experiment was not as high as those quoted by Sheer and Eckert.

6.1.6 Temperature of Plasma Arc

One of the most difficult problems faced in describing the properties of the plasma jet concerns the measurement of the plasma temperature. A direct measuring device is not usually satisfactory, because of high temperature which can be expected even in a low power generator. The use of ordinary high temperature direct measuring techniques is out of question unless considerable cooling is used -

this means usually a bulky probe which will cause severe flow disturbance in a small jet.

An indirect measuring device involves a spectroscopic technique, the use and the description of the technique are beyond the scope of the present report. References 24, 28 and 29 provide recent examples of this technique applied to the temperature measurement in plasma jets. However, the temperature of the plasma arc can still be estimated by considering the efficiency of the plasma generator, the gas flow rate which can be measured, the degree of ionization, and other appropriate assumptions. Then Saha's equation can be used to solve for the equilibrium temperature. The appropriate assumptions for the use of this equation include

(i) the energy in the plasma will be used completely to ionize the neutral gas atoms,

(ii) equilibrium conditions must exist,

(iii) at equilibrium, the particles must possess a Maxwell-Boltzmann's distribution - the mean kinetic energy would correspond to the equilibrium temperature, and

(iv) the argon atom will be only singly ionized.

Based on the above assumptions and the efficiency of the plasma generator used in the experiment, the temperature of the plasma arc was found to be approximately 9,900°K at 1.6 kw and 10,100°K at 2.0 kw power input. These figures undoubtedly represented the maximum arc temperatures. Knipe, Stokes and Streng (21) reported arc temperatures of 9,000°K at 2 kw and 19,000°K at 14 kw power input, based on an argon gas flow rate of 16 litres/min. and an energy transfer efficiency of 56%.

6.2 Bulk Heat Transfer Measurements

The heat transfer rate at the water-cooled copper anode has been found to be approximately 375,000 BTU/hr.ft^2. With a large cooling water flow rate, the temperature of the surface actually in contact with the plasma jet can be kept much below its melting point. This indicates the possibility of a future study in heat transfer with an extreme temperature difference and a very high heat transfer rate.

Along the heat exchanger, the upper wall temperatures differed from the bottom wall temperatures located diametrically opposite, by as much as 23% at the inlet while further along the heat exchanger, the differences were about 5%, although the water flow rate in each section in the annular passage was maintained constant. These differences show the slight assymetry of the plasma jet with respect to the inner tube of the heat exchanger and reveal the presence of free convective heat transfer especially near the inlet. As mentioned earlier, the plasma jet exhibited a random fluctuation and this fluctuation was superimposed on the "steady-state" readings, causing a uniform fluctuation in the gas bulk temperatures and the wall temperatures.

The copper-constantan thermocouples measuring the wall temperatures were carefully checked for faulty installations and connections which might have caused the differences in the opposite wall temperatures of heat exchanger. The dry inner tube was heated with a propane torch and then cooled in air. The consistent transient response of the opposite pairs indicated the absence of any erratic thermocouples.

The experimental results of the heat transfer measurements are plotted in Figures 16, 17 and 18. The results show several interesting features about the heat transfer characteristics of the present system. For example, in Figure 18, the graph showing the Nusselt number as a function of the non-dimensional tube length $x/D/Re_x Pr$ may be divided into three regions.

The first part consists of the positive slope of the curve from $x/D/Re_x Pr = 0$ to approximately $x/D/Re_x Pr = 3.5$. The second part consists of the sharp drop of the Nusselt number while the last part of the curve once again exhibits a positive slope for the Nusselt number. The following explanation is given of these three regimes.

Since the diameter of the inner tube (1.430") of the heat exchange is approximately 2.3 times larger than the initial diameter of the plasma jet, it is expected that at the inlet of the heat exchanger the plasma jet resembles a free-jet. This resemblance continues down the tube until the jet spreads far enough to be affected by the cold wall boundaries.

During the initial start-up of the test, the inner tube of the heat exchanger is filled with air which will be mixed with the hot gas stream and quickly exhausted leaving only argon in the system. It is suggested that in the inlet length which the jet takes to spread to the wall, a vortex pattern will exist in the stagnation region between the jet and the wall causing a back-flow near the entrance. The vortex pattern gives rise to some distinct eddies transferring some energy from the hot boundaries of the jet to the cold wall.

Superimposed on this eddy formation will be the effect of free convective heat transfer. The extremely hot plasma jet provides large temperature differences combined with low axial velocity and it may be that on the top of the tube, the eddy formation is suppressed entirely by the vertically rising gases. This flow pattern which forms almost a horse-shoe about the jet, and the one as described in the last paragraph, present a complicated system in heat transfer. However, it may serve to explain in part the differences in wall temperatures observed near the inlet.

What appears to be the free convection can actually be observed through the window at the exhaust end of the heat exchanger. The light from the plasma arc combined with the strong heating effect of the plasma jet produce severe changes in the index of refraction of the gas medium (shadowgraph technique) and one can see the gas rising above the jet, similar to that from a heated plate in stagnant air.

The presence of free convection is also upheld by the experimental evidence. For example, the correlation of the local Nusselt number and the Rayleigh number (Gr Pr) compares favourably with that presented by McAdams (27) as $Nu = 0.53\ Ra^{1/4}$. The comparison can be seen in Figure 18b. Higher local heat transfer coefficients were obtained in the experiment. Although the Grashof numbers along the inlet length have been calculated to be far below 10^8, which demonstrate laminar flow in free convection, the effect of turbulent flow is obvious. The cause of the turbulent flow is believed to be the combined effect of the turbulent eddies due to the entrainment of the gas into the emerging jet, the probable back-flow and the basic free convection process.

Argon, being a monatomic gas, is transparent to thermal radiation, i.e., it will not emit nor absorb any appreciable amount of radiation until ionization of the gas becomes significant. Therefore it follows that at the inlet of the heat exchanger, the thermal radiation is negligible, except that some may have come from the heated electrodes. This source of radiation has been estimated to be negligibly small (see Appendix B). Hot carbon particles from the cathode erosion are also probable sources of radiation. However since the erosion rate (0.012 gm./min.) only amounts to approximately 0.1% of the gas flow rate (122 gm./min.), this source of heat transfer is considered small enough to be neglected.

When the jet boundaries have spread as far as the wall, the convective heating of the wall by the fluid stream begins. The transition between the two modes of heat transfer is quite distinct. Coinciding with this transition is the region of entrance effects, in which the velocity and temperatures are being established. As seen in Figure 18a, the transition is also accompanied by a sharp fall of the local heat transfer coefficient and hence the local Nusselt number.

Since the entrance length depends on the jet configuration, temperature ratio, and free stream turbulence, it can only be approximated for the configuration at hand. A precise determination of the thermal length requires a calculation or measurement of the thermal boundary layer. Sometimes, it may be simpler to determine the distance required for either the local Nusselt number or the local heat transfer coefficient to reach a constant value as a function of x/D. However, with high gas-to-wall temperature differences and for fluids whose physical properties vary appreciably with temperature, the local

Nusselt numbers cannot be a reliable criterion for establishing the thermal entrance length.

After the transition, the local Nusselt numbers continue to increase slightly in the direction of flow. Apparently the increase in Nu_x is due to the decrease in the thermal conductivity of argon with the local film temperature. On the other hand the local heat transfer coefficients appear to increase slightly with the axial distance (Figure 17a, b). As a result, it is believed that the rates of changes for both h_{gs} and k_{gf} are not the same.

Another interesting phenomenon directly concerned with the high temperature difference and the low velocity of the gas flow, appears in the determination of whether the flow is laminar or turbulent in the stabilized region. The Reynolds numbers ($\angle$ 1400) based on the bulk temperatures are far below 2100 while those based on the film temperatures go over 2100 at approximately 9 diameters. If the critical Reynolds number is assumed to be 2100, the nature of the flow in the central core is laminar while it is turbulent in the region enveloping the core. Other experimenters (20) have studied similar problems and found out that the resulting flow was actually laminar. In Figure 18a the consistent increase of the Nusselt number in the direction of the flow after the thermal entrance length is established, indicates the presence of laminar flow.

The heat flux at each station from the hot gas does not agree very well with the energy gained by the cooling water at the same station. It is believed that the difference is due to the measurement of the gas temperatures. The peak gas temperatures were more likely to be measured than the average gas temperatures.

7. RECOMMENDATIONS

From the above study, a few things may be pointed out for further improvement in plasma generator design and high temperature heat transfer work.

A higher efficiency and a higher gas exit velocity are both desirable properties of a plasma generator. These can be obtained if the water-cooled copper electrode is replaced by a thoriated tungsten one having a smaller central hole, and the transpiration-cooled electrode can then be used as the anode, the erosion rate of which is negligible.

The temperature profile of the plasma jet is a matter of interest to many. With a steady jet, it can be estimated by the spectroscopic methods as described by Knopp (28) and Weiss (4). An increase in the d.c. power input would produce higher plasma temperatures. It is believed that with a stronger external electric field and a heavier arc starter, some diatomic gases may be used as the transpiration fluids, thus lowering the operation cost of the experiment.

When a hotter plasma jet is obtained, high temperature heat transfer studies may be performed with extreme temperature differences, with the plasma jet impinging on any shape of a water-cooled body, or forcing through a short, narrow water-cooled passage. These studies have important practical applications in chemical synthesis, in which it is often necessary to cool high temperature gases rapidly; in space re-entry simulation problems and in various other fields.

8. CONCLUSION

Preliminary experiments on the original plasma generator have led to some modifications of the design, in particular the reversal of the electrode polarity and the introduction of a water-cooled copper anode. The experimental study of the performance characteristics has produced some informative results on the modified configuration, which has a few merits to be mentioned. They include the steady arc operation at high gas flow rates, low cathode erosion rate, clean plasma jet and the easy accessibility of the jet for further study.

The heat transfer measurements from the high temperature gas have demonstrated several interesting phenomena, largely due to the high temperature differences and the low velocity of the gas flow. The average values of the local heat transfer rates and the local heat transfer coefficients as found, are of definite interest in further related heat transfer studies of the plasma jet.

The temperatures of the stainless steel wall have been measured to be under $70^{o}F$. Boiling heat transfer and related phenomena were not observed. As a result, the parallel-cocurrent-flow heat exchanger and the instrumentation will enable similar heat transfer measurements from a "hotter" and perhaps a "bigger" plasma jet.

9. NOMENCLATURE

Symbol	Description	Units
A	Surface area	ft^2
A_a	Heat transfer area at anode	ft^2
A_c	Cross-sectional area	ft^2
A_i	Heat transfer area at each station, based on the inner radius	ft^2
C_p	Specific heat	$BTU/lb_m\ ^oR$
C_{pw}	Specific heat of cooling water	$BTU/lb_m\ ^oR$
C_{pg}	Specific heat of gas	$BTU/lb_m\ ^oR$
D,d	Diameter	ft
D	Inside diameter of inner tube	ft
d_a	Diameter of the central hole of the anode	ft
d_t	Diameter of the electrically welded thermocouple junction	ft
g	Gravitational constant	ft/sec^2
h	Convective heat transfer coefficient	$BTU/hr.ft^2\ ^oR$
h_{gt}	Average convective heat transfer coefficient between the hot gas and the thermocouple junction	$BTU/hr.ft^2\ ^oR$

h_{gs}	Local convective heat transfer coefficient between the hot gas and the tube wall	$BTU/hr.ft^2\ {}^oR$
I	Arc current	amperes
k	Thermal conductivity	$BTU/hr.ft^oR$
k_{ss}	Thermal conductivity of the stainless steel tube	$BTU/hr.ft^oR$
k_g	Thermal conductivity of argon;	
	k_{gb} - Thermal conductivity of argon evaluated at the bulk temperature	$BTU/hr.ft^oR$
	k_{gf} - Thermal conductivity of argon evaluated at the mean film temperature	
K	Boltzmann Constant 1.38×10^{-23}	$joule/{}^oK$
L	Overall length of the heat exchanger	ft
ℓ_a	Width of the heat transfer area at the anode	ft
m	Mass flow rate	lb_m/hr
m_g	mass flow rate of argon	lb_m/hr
M_g	Mass flow rate of argon	kg-mole/sec
m_w	Total mass flow rate of cooling water for the annular passage	lb_m/hr
m_{wa}	Mass flow rate of cooling water for the anode	lb_m/hr
m_{wc}	Mass flow rate of cooling water for the cathode	lb_m/hr
N	Avogadro's number 6.023×10^{26}	$\frac{molecules}{kg\text{-}mole}$
P	Power input of the plasma arc	kilowatts
p	Ambient pressure	atm.

Q	Heat transfer rate	BTU/hr
Q_{ra}	Heat lost by radiation at the anode	BTU/hr
Q_{wa}	Heat transfer rate to anode cooling water	BTU/hr
Q_{wc}	Heat transfer rate to cathode cooling water	BTU/hr
q_g	Heat balance of the hot gas	BTU/hr
q_w	Heat balance of cooling water in the annulus	BTU/hr
T,t	Temperature	^oF or ^oR
t_1	Inlet temperature of cooling water for electrodes	^oR
t_2	Outlet temperature of cooling water for anode	^oR
t_3	Outlet temperature of cooling water for cathode	^oR
T_a	Melting point of copper	^oR
T_E	Equilibrium temperature	^oK
T_{gb}	Mean gas bulk temperature at $x + \frac{1}{2}\Delta x$ $T_{gb} = \frac{1}{2}\left[T_x + T_{x+\Delta x}\right]$ calculated	^oR
T_{gc}	Mean centerline gas temperature	
T_{gf}	Local film temperature $T_{gf} = \frac{1}{2}\left[T_{gb} + T_{ss}\right]$	
T_{ss}	Wall temperature	
T_{tx}	Apparent ℄ gas temperature as registered by thermocouple	^oR
t_{wb}	Mean water bulk temperature at $x + \frac{1}{2}\Delta x$ $t_{wb} = \frac{1}{2}\left[t_x + t_{x+\Delta x}\right]$	^oR
t_x	Water bulk temperature at x	^oR

$t_{x+\Delta x}$	Water bulk temperature at $x + \Delta x$	^oR
T_x	Corrected C gas bulk temperature at x	^oR
$T_{x+\Delta x}$	Corrected gas bulk temperature at $x + \Delta x$	^oR
u_I	First level ionization potential of argon	electron volts
V	Arc voltage	volts
x	Distance (axial) along the tube	ft

Greek Symbol	Description	Units
β	Bulk modulus of argon gas	$^oF^{-1}$
ε_c	Emissivity of hot copper anode	-
ε_t	Emissivity of welded thermocouple junction	-
η	Efficiency of the plasma generator	%
ρ	Density of argon gas	lb_m/cu.ft.
μ	Dynamic viscosity	lb/ft.hr.
ν	Kinematic viscosity	ft^2/hr
ϕ	Degree of ionization	-
σ	Stefan Boltzmann constant	$BTU/ft^2hr^oR^4$

Dimensionless Parameters	Description	Units
Nu	Nusselt number ($Nu = \frac{hD}{k}$)	-
Re	Reynolds number $Re = \frac{mD}{A_c\mu}$	-
Pr	Prandtl number $Pr = \frac{C_p\mu}{k}$	-
Gr	Grashof number $Gr = \frac{\beta g D^3 \Delta T}{2}$	-

Letter Subscripts	Description	Units
a	Anode	-
c	Cross-section	-
E	Equilibrium	-
g	Gas	-
gb	Gas bulk temperature	-
gc	Gas center-line temperature	-
gf	Gas film temperature = ½ $T_x + T_{ss}$	-
gs	From gas to stainless steel wall	-
gt	From gas to thermocouple junction	-
i	Station on stainless steel tube surface	-
I	First-level	-
ra	Radiation at the anode	-
ss	Stainless steel	-
t	Thermocouple	-
tx	Measured gas temperatures	-
w	Cooling water for annulus	-
w_a	Cooling water for anode	-
w_c	Cooling water for cathode	-
w_s	From cooling water to the stainless steel wall	-
x	Temperature at x from inlet	-
$x + \Delta x$	Temperature $x + \Delta x$ from the inlet	-
1	Inlet water temperature at anode and cathode	-
2	Outlet water temperature at anode	-
3	Outlet water temperature at cathode	-

10. REFERENCES

1. Compton, K. T. and I. Langmuir, "Electrical Discharges in Gases", Part I, Survey of Fundamental Processes, Rev. of Modern Physics, Vol. 2, No. 2, pp. 123-242, April 1930.

2. Somerville, J. M., "The Electric Arc", Methuen and Co. Ltd., London, England, John Wiley and Sons Inc., New York, 1959.

3. Francis, G., "Ionization Phenomena in Gases", Butterworths Scientific Publications, London, England, 1960.

4. Weiss, R., "Unterschung des Plasmastrahles, der aus einen Hochleistungsbogen Austritt", Li, J. S., E. O. Gadamer English Translation, McMaster University, 1964.

5. Finkelnburg, W. and H. Maecker, "Gas Discharges", Handbuch der Physik XXII, Berlin, Springer Verlag, pp. 254-444, 1956.

6. John, R. R. and W. L. Bade, "Recent Advances in Electric Arc Plasma Generator Technology", ARS Journal, Vol. 31, No. 1, 1961.

7. Fischer, H. and L. C. Mansur, "Conference on Extremely High Temperatures", John Wiley and Sons, New York, Chapman and Hall Ltd., London, 1958.

8. Schoeck, P. A. and E. R. G. Eckert, "Experiments on the Transpiration Cooled Anode in an Electric Arc", Proceedings of Heat Transfer and Fluid Mechanics Institute, Stanford University Press, 1961.

9. Sheer, C., J. A. Cooney, F. R. Sileo and Rothacker, "Effect of Fluid Transpiration Through the Anodic Arc Boundary", Vitro Laboratories, West Orange, N. J., U. S. A., 1961.

10. Dooley, M. T., W. K. McGregor, and L. E. Brewer, "Characteristics of the Arc in a Gerdien-Type Plasma Generator", ARS Journal, Vol. 32, September 1961.

11. Perlmutter, M. and R. Siegel, "Heat Transfer by Combined Forced Convection and Thermal Radiation in a Heated Tube", Journal of Heat Transfer, ASME Transactions, November 1962.

12. Zellnick, H. E. and S. W. Churchill, "Convective Heat Transfer From High Temperature Air Inside a Tube", A.I.Ch.E. Paper No. 57-HT-33, 1957.

13. Deissler, R. G., "Turbulent Heat Transfer and Friction in the Entrance Regions of Smooth Passages", Trans. A.S.M.E., Vol. 77,p1221, 1957.

14. Pinkel, B., "A Summary of NACA Research on Heat Transfer and Friction for Air Flowing Through Tube with Large Temperature Difference", Trans. A.S.M.E., Vol. 74, pp. 305-317, 1954.

15. Deissler, R. G., "Investigation of Turbulent Flow and Heat Transfer in Smooth Tubes, Including the Effects of Variable Physical Properties", Trans. A.S.M.E., Vol. 73, pp. 101-107, 1951.

16. Wolf, H., "Heating and Cooling Air and Carbon Dioxide in the Thermal Entrance Region of a Circular Duct with Large Gas to Wall Temperature Differences", Journal of Heat Transfer, Vol. 81, Series C, No. 4, November 1959.

17. Wilkinson, J. B., and D. R. Milner, British Welding Journal, p. 115, February 1960.

18. Nestor, O. H., "Experimental Determination of Current Density and Heat Transfer Intensity Distribution at the Anode of High Current, Inert Gas Arcs", Ph.D. Thesis, University of Buffalo, Buffalo, New York, 1960.

19. Schoeck, P. A., "An Investigation of the Anode Energy Balance of High Intensity Arcs in Argon", Modern Developments in Heat Transfer, Warren Ibele, Academic Press, New York, 1963.

20. Emmons, H. W., "Recent Developments in Plasma Heat Transfer", Modern Developments in Heat Transfer, Warren Ibele, Academic Press, New York, 1963.

21. Stokes, C. S., W. W. Knipe, and L. A. Streng, "Heat Transfer Rates of an Argon Plasma Jet", Journal of Electrochemical Society, Vol. 107, pp. 35-38, January 1960.

22. Reed, T. B., "Heat Transfer Intensity in Induction Plasma Flames and Oxy-hydrogen Flames", Lincoln Laboratory, M.I.T., Lexington, Massachusetts, U. S. A.

23. Wethern, R. J. and R. S. Brodkey, "Heat and Momentum Transfer in Laminar Flow: Helium Initially at Plasma Temperatures", A.I.Ch.E. Journal, Vol. 9, No. 1, January 1963.

24. Cambel, A. B., "Plasma Physics and Magnetofluidmechanics", McGraw-Hill, New York, N. Y., 1963.

25. Kreith, F., "Principles of Heat Transfer", International Textbook, 1962.

26. Hilsenrath, J. and Y. S. Touloukian, "The Viscosity, Thermal Conductivity, and Prandtl No. for Air, O_2, N_2, NO, H_2, CO, CO_2, H_2O, H_e and A", Trans. A.S.M.E., p. 967, 1954.

27. McAdams, W. H., "Heat Transmission", 3rd ed., McGraw-Hill, New York, 1954.

28. Knopp, Chad, Gottschlich and Cambel, "The Spectroscopic Measurement of Temperature in Transparent Argon Plasma", J. of Quant. Spectrosc. Radiat. Transfer, Vol. 2, pp. 297-299, 1962.

29. Loth, J. L., "Thermal Radiation Energy Transfer from Very High Temperature Plasmas", Ph.D. Thesis, Department of Mechanical Engineering, University of Toronto, Toronto, Ontario, 1962.

30. Keenan and Keyes, "Thermodynamic Properties of Steam", John Wiley and Sons Inc., 1936.

31. Cobine, J. D., "Gaseous Conductors", McGraw-Hill, New York, 1941.

32. Butler, R. and E. Kerr, "An Introduction to Numerical Methods", Sir Isaac Pitman and Sons, London, 1962.

11. ILLUSTRATIONS

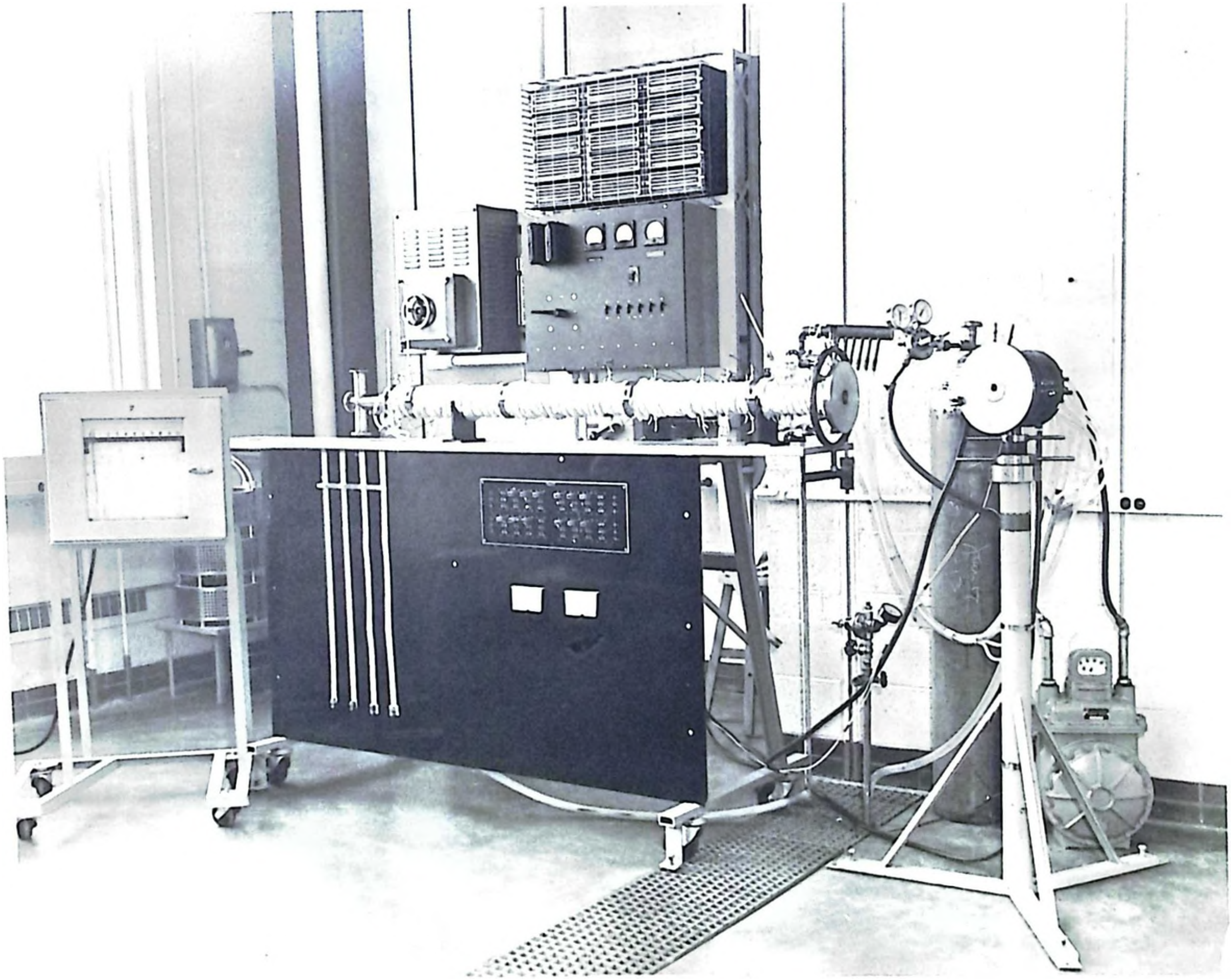

FIGURE I TEST EQUIPMENT ASSEMBLY

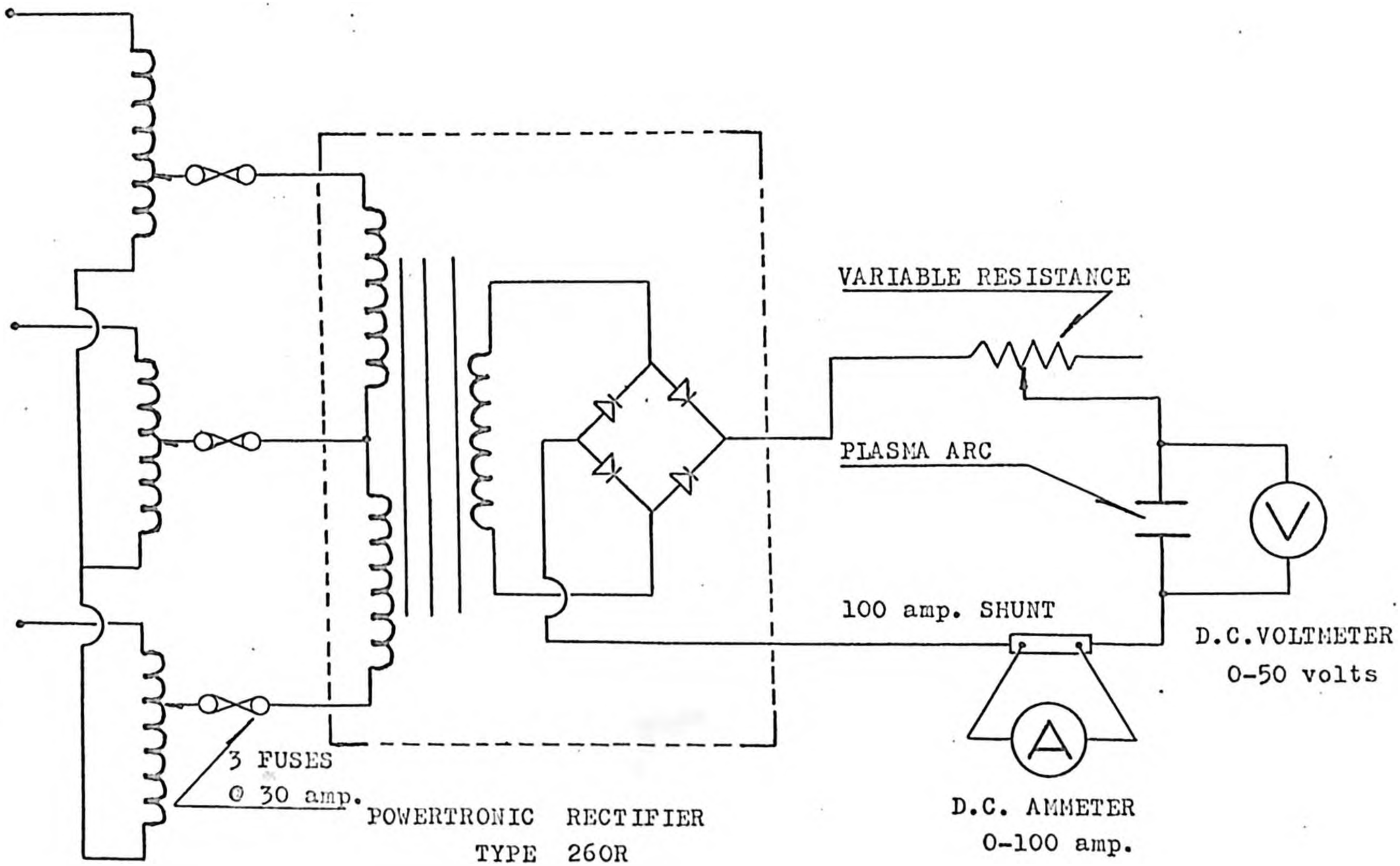

THE SUPERIOR
ELECTRIC POWERSTAT
INPUT 575 volts
3 phase 60cps.
OUTPUT 0-575 volts
max. current 28 amp.

INPUT 575 v. 14.6 amp.
3 phase 60 cps
OUTPUT 110 d.c. volts
91 d.c. amp.

FIGURE 2 POWER SUPPLY CIRCUIT

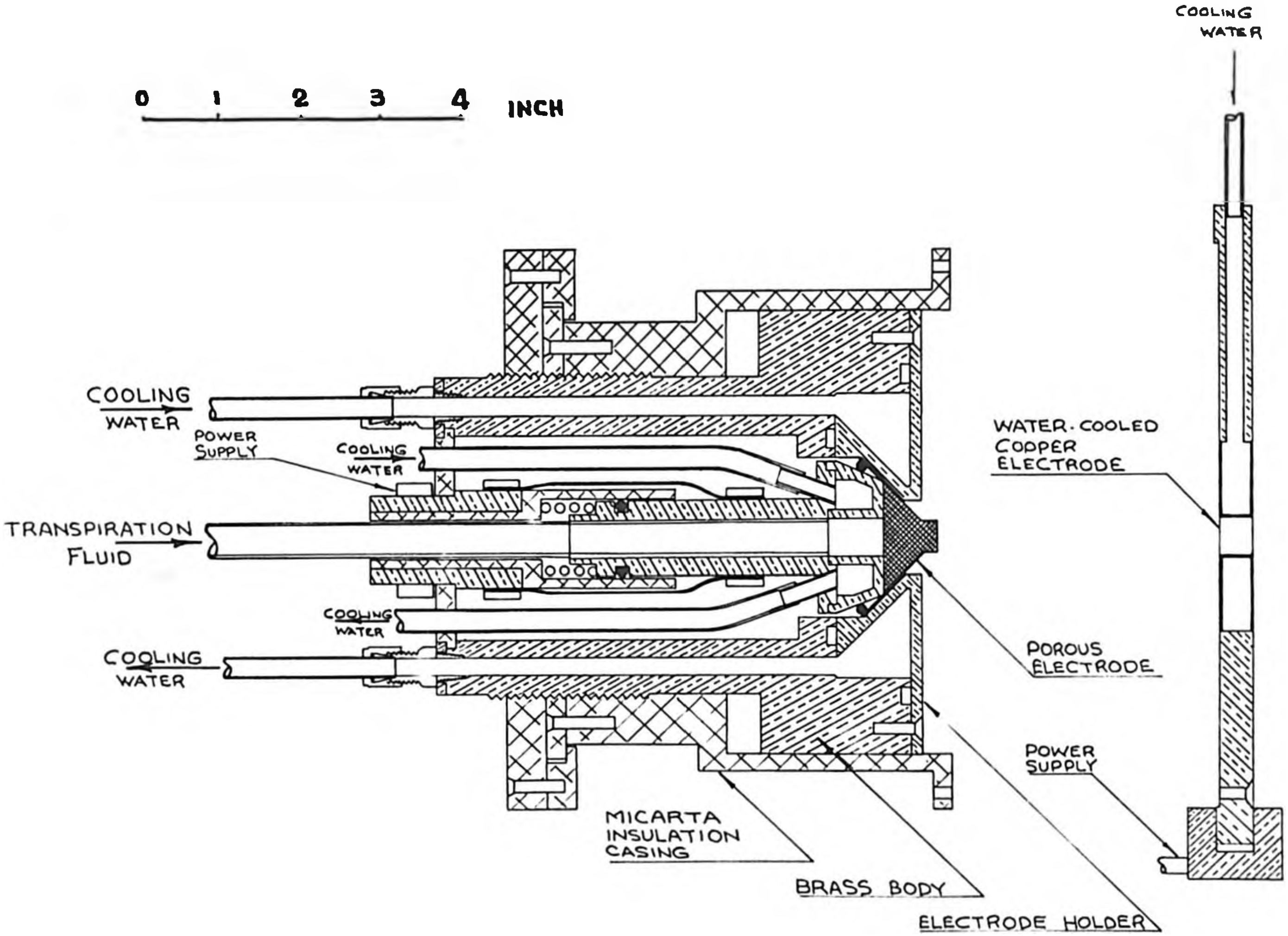

FIGURE 3 CROSS-SECTIONAL VIEW OF PLASMA GENERATOR ASSEMBLY

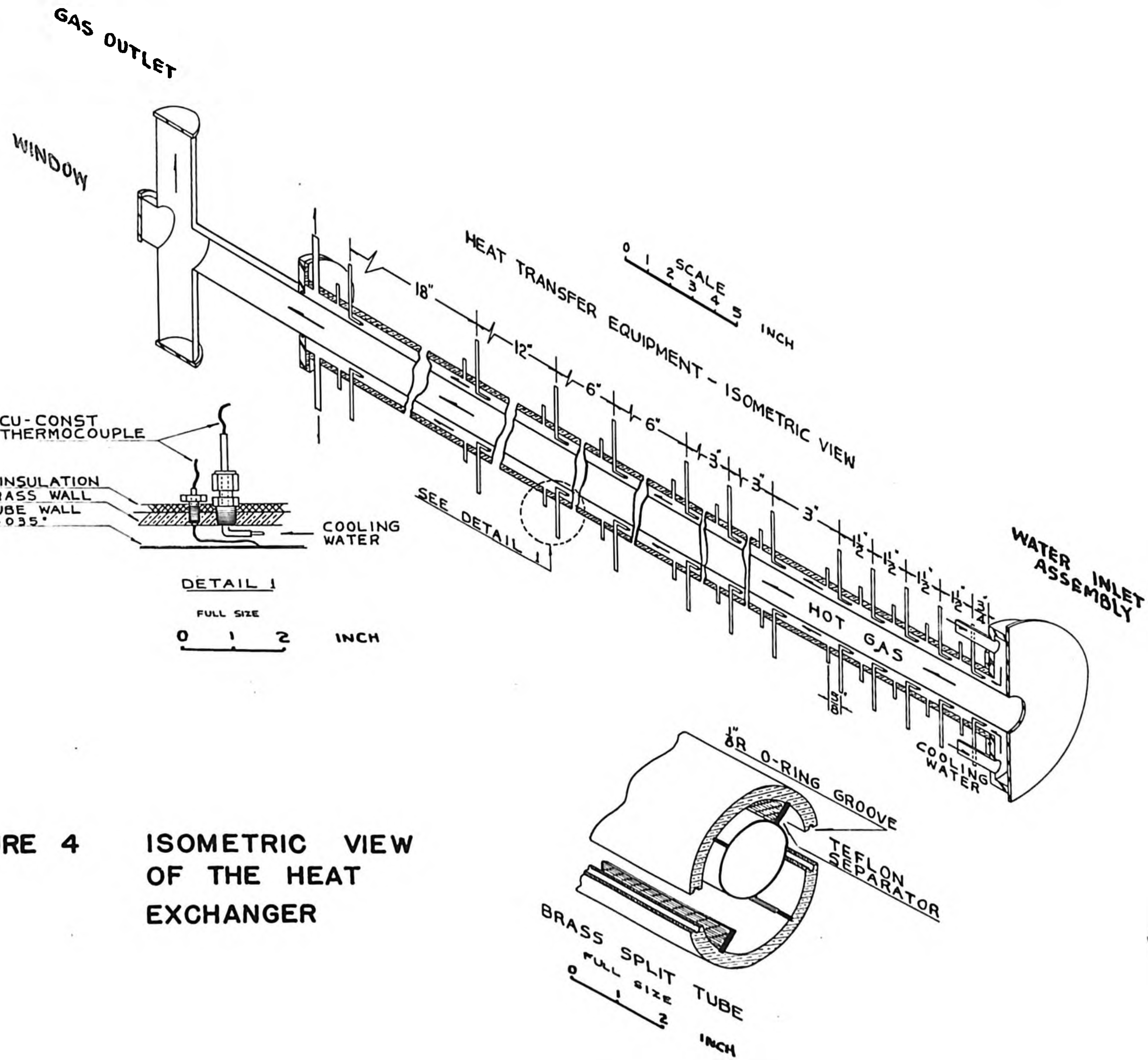

FIGURE 4 ISOMETRIC VIEW OF THE HEAT EXCHANGER

FIGURE 5a BRASS SPLIT TUBE

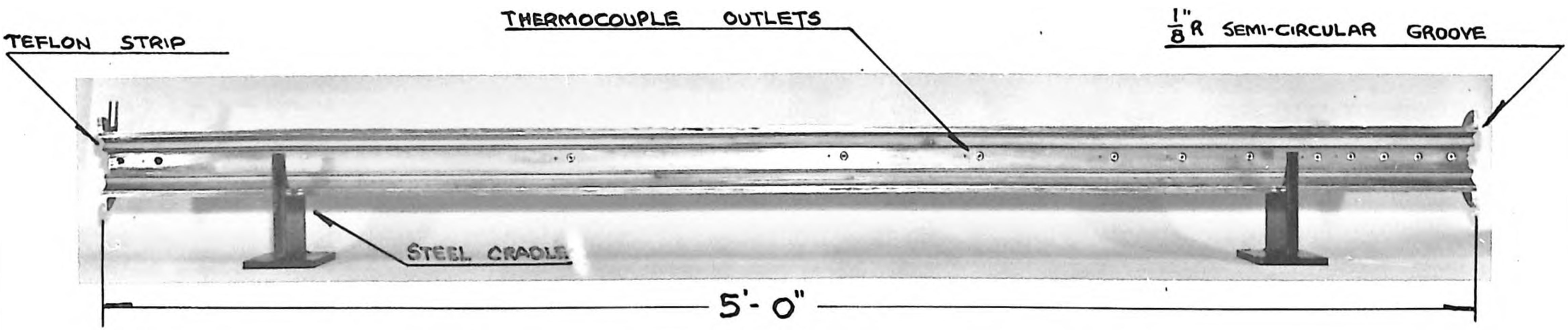

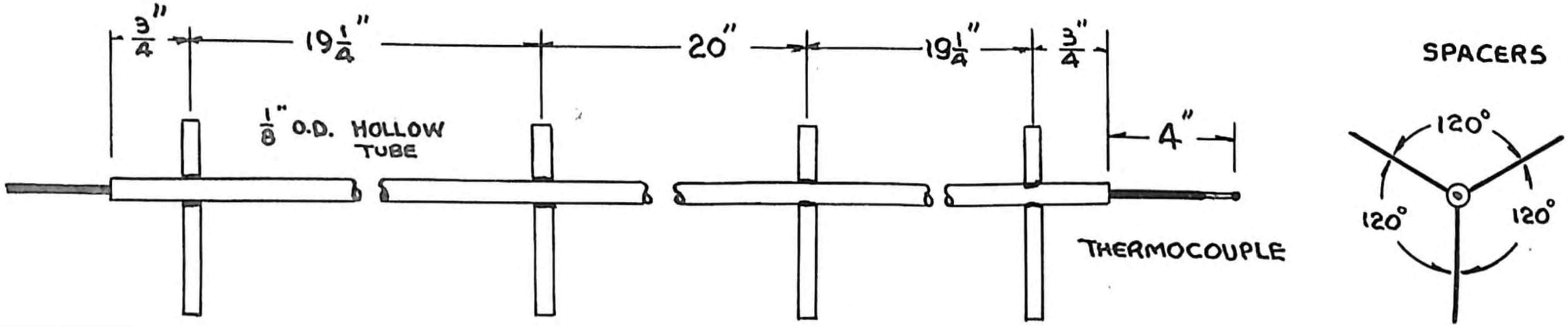

FIGURE 5b TEMPERATURE PROBE

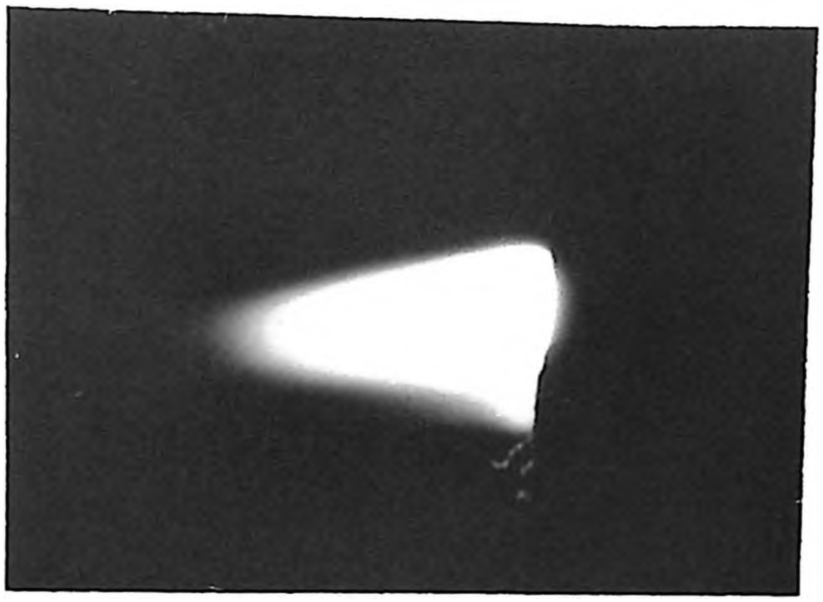

SYMMETRICAL PLASMA JET WITH
CATHODE IN GOOD CONDITION

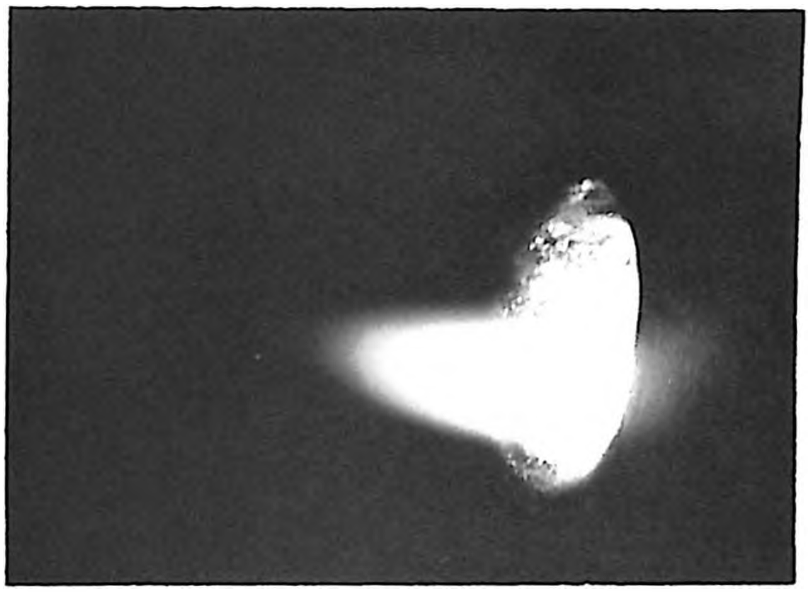

SKEWED JET WITH WORN-OUT CATHODE
AFTER ABOUT 90 MINUTES OF OPERATION.
THE WORN-OUT CATHODE IS SHOWN IN
FIGURE 11B.

WATER-COOLED COPPER ANODE; NC50 GRAPHITE POROUS CATHODE;
GAS FLOW RATE = 122 GM./MIN.; ARC POWER INPUT = 1.780 KW.;
ARC GAP DISTANCE = 1/16 INCH.

FIGURE 6 PLASMA JET

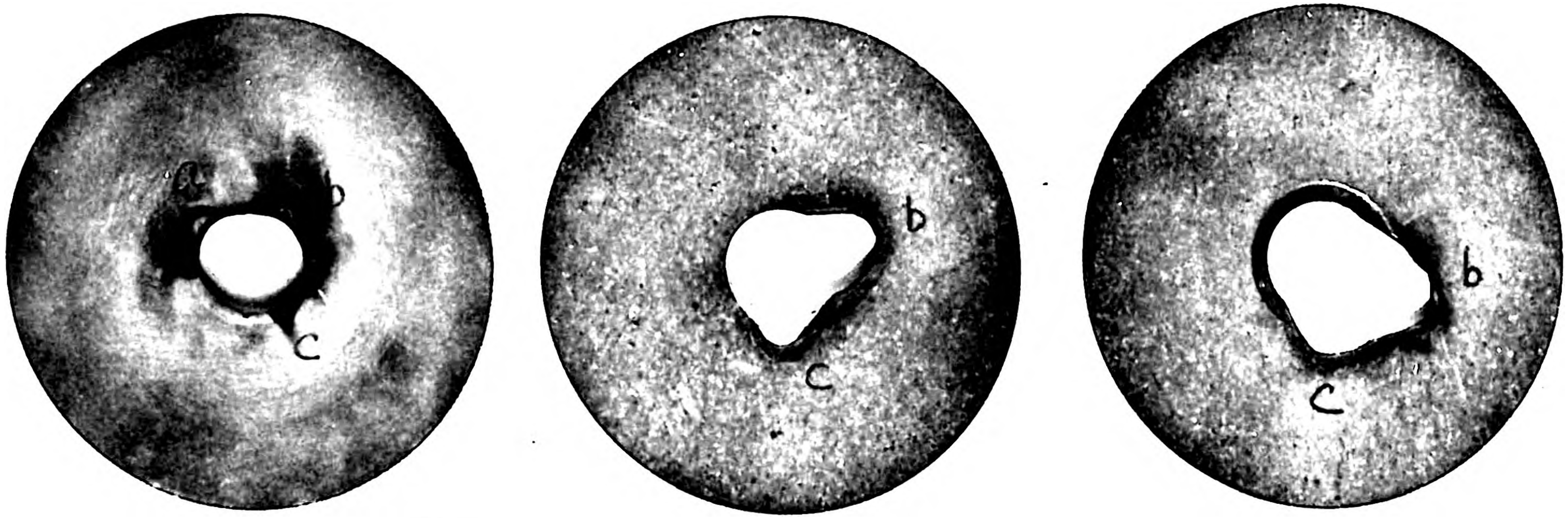

AUC CARBON (i)

ATJ CARBON (ii)

COMMERCIAL CARBON (iii)

(i) At the start, the cathode spot oscillated between a, b and c

(ii) After 10 - 15 minutes, the cathode spot oscillated between points b and c only

(iii) After 15 - 20 minutes, erosion at b and c continued. Finally the cathode spot stayed either at b or c, and a skewed plasma jet resulted. At higher gas flow rate, the cathode spot was blown off and the operation interrupted.

FIGURE 7 ERODED CARBON DISK CATHODES

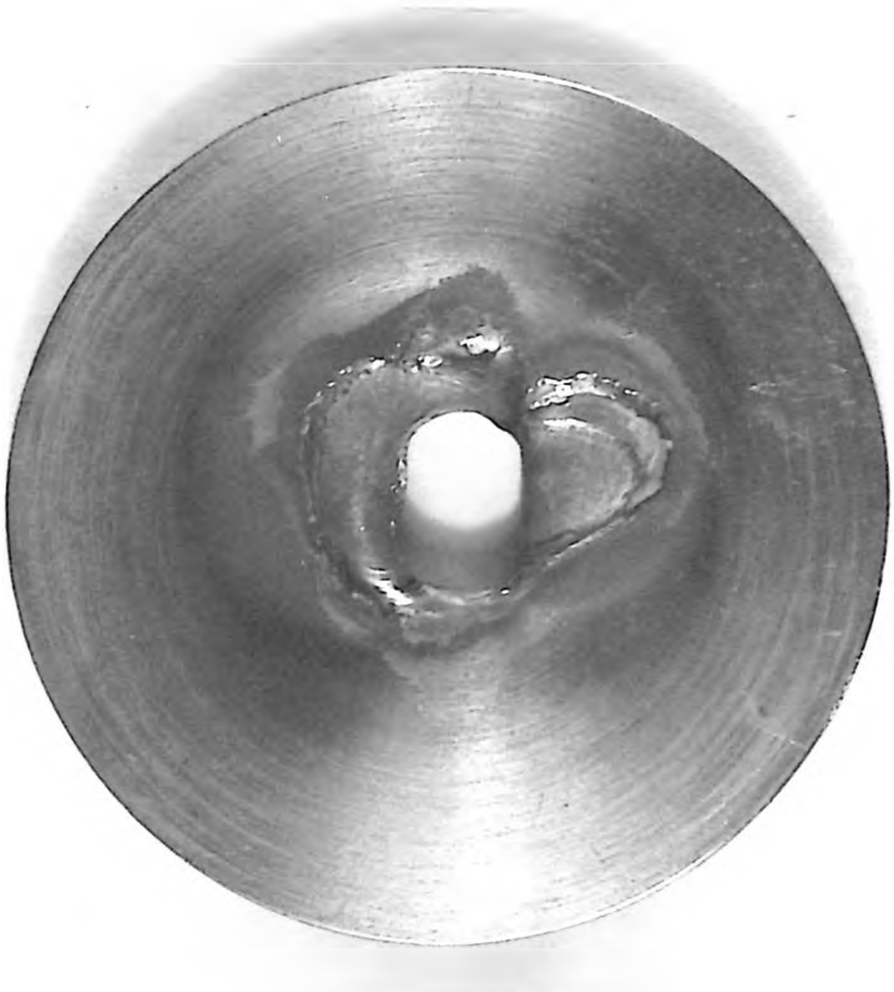

FIGURE 8 ERODED INCONEL CATHODE
(EXAMPLE OF COLD CATHODE)

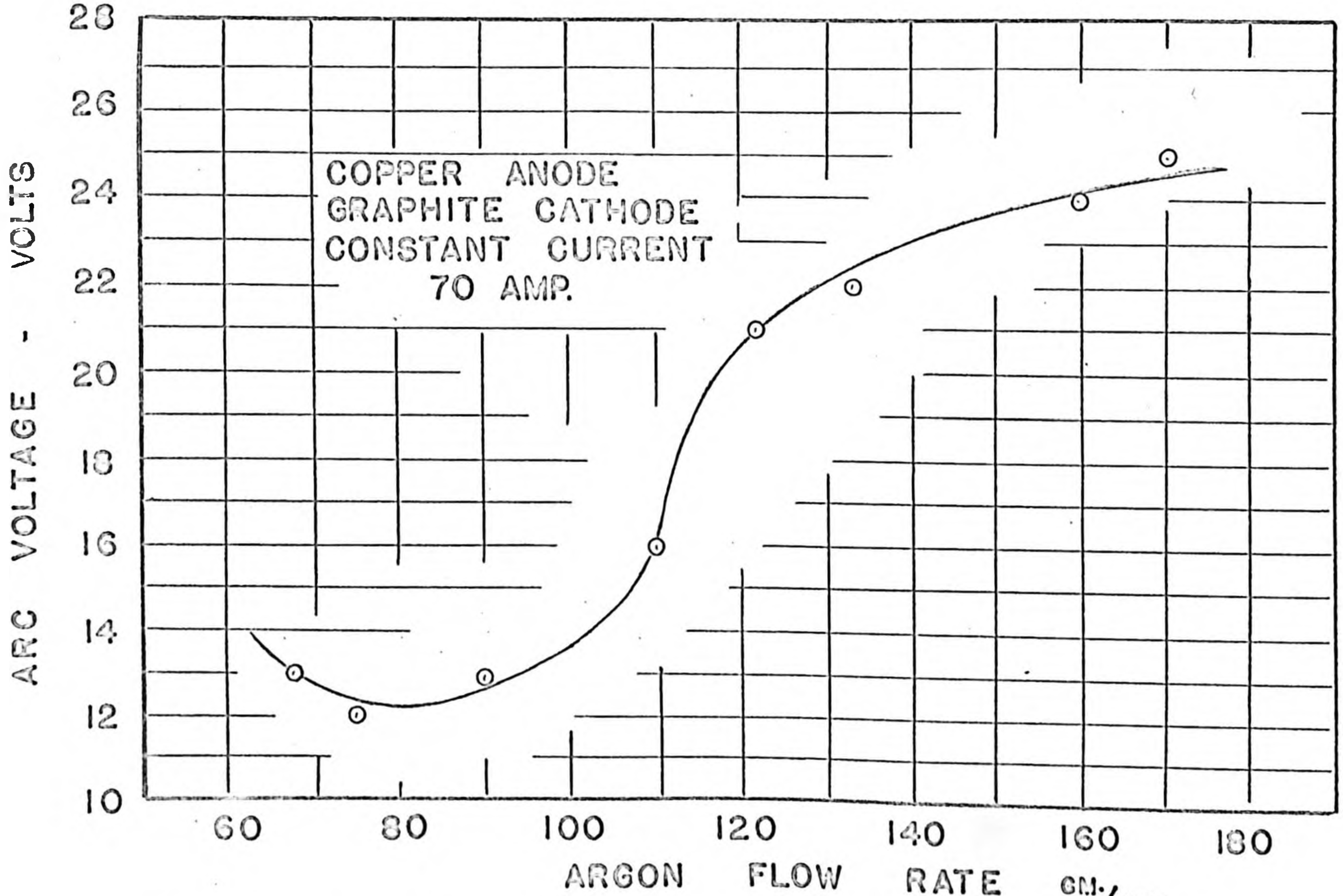

FIG. 9 EFFECT OF ARGON FLOW RATES ON ARC VOLTAGE

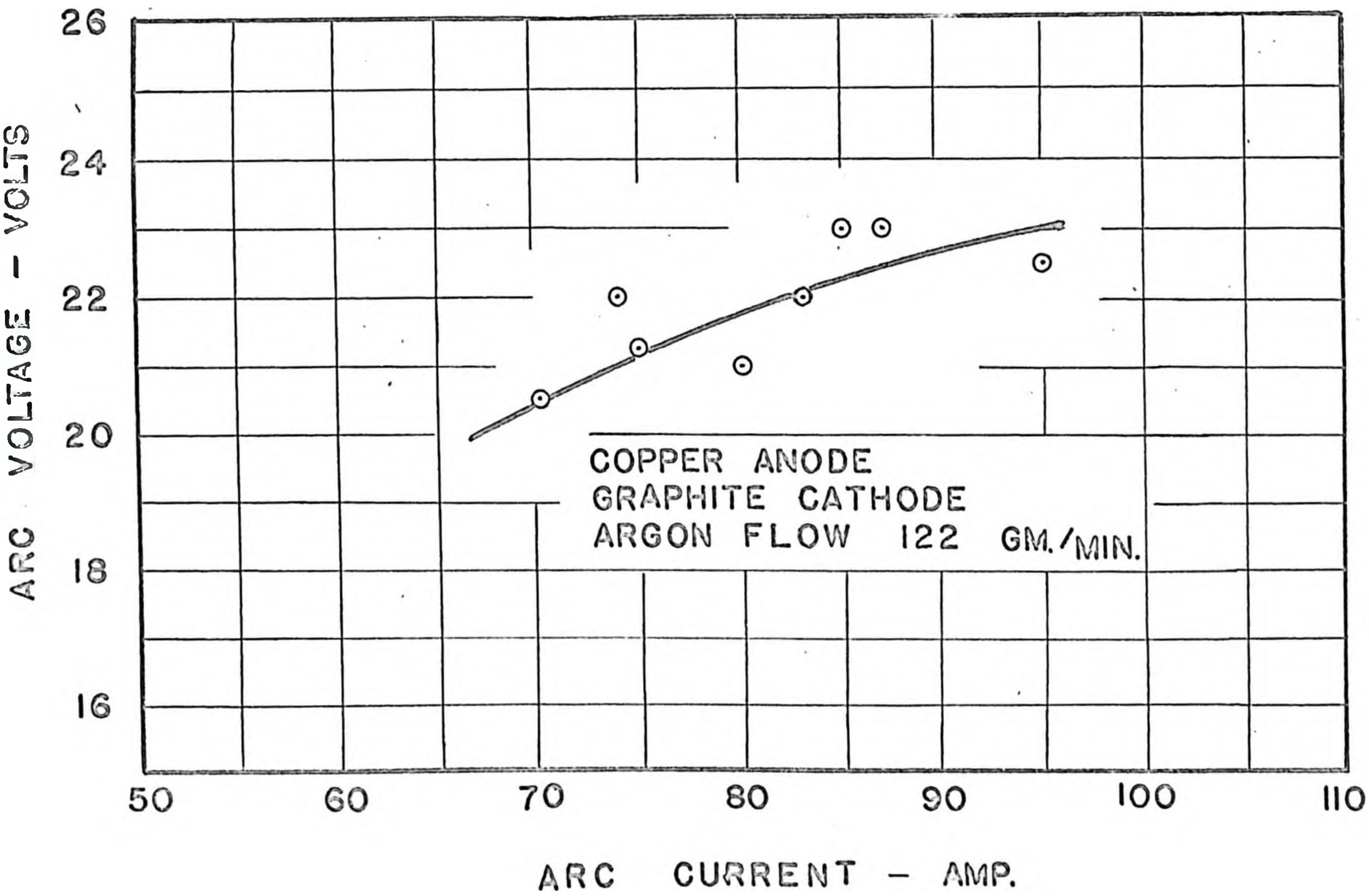

FIG. 10 CURRENT - VOLTAGE CHARACTERISTICS

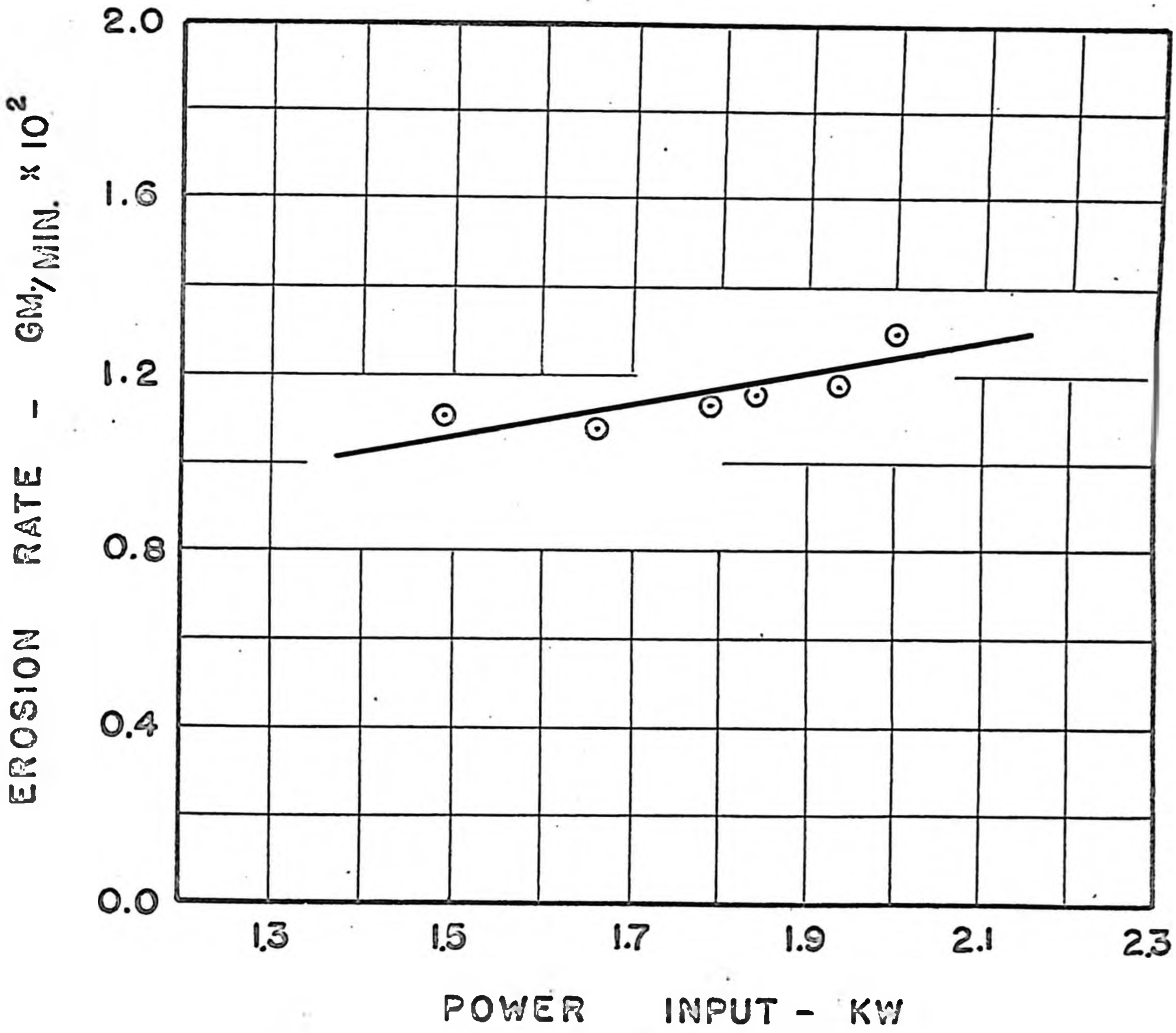

FIG. 11a CATHODE EROSION RATE
NC50 GRAPHITE CATHODE

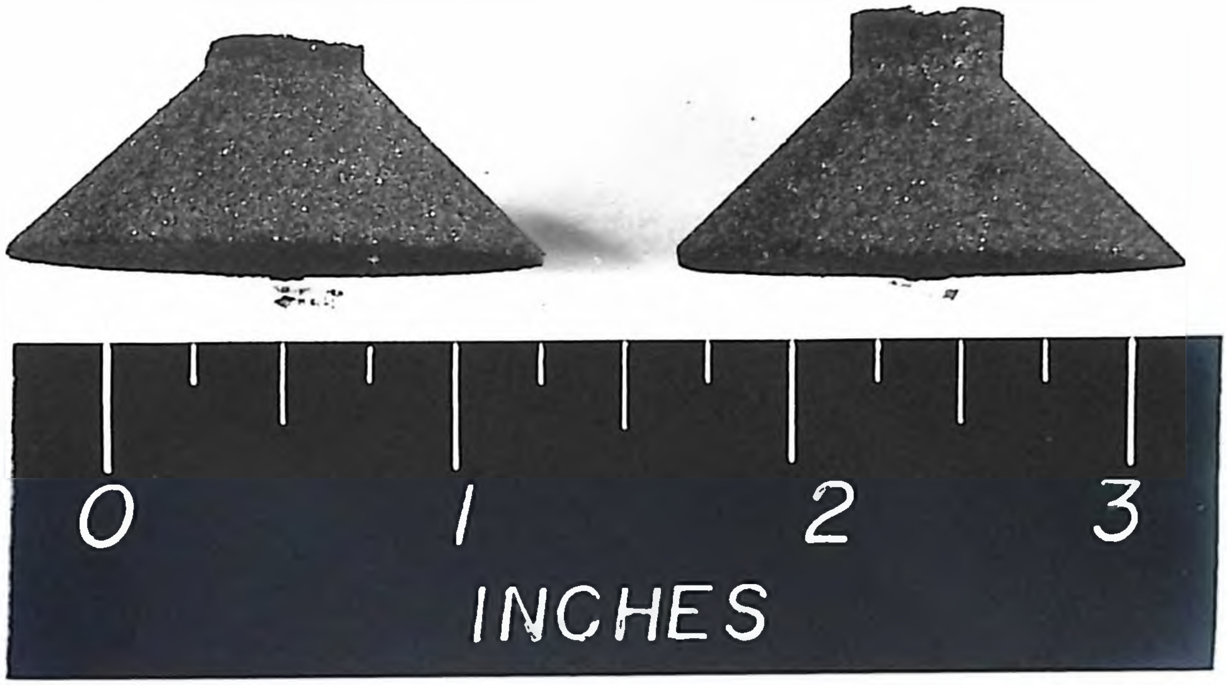

FIGURE 11B ERODED POROUS CATHODES

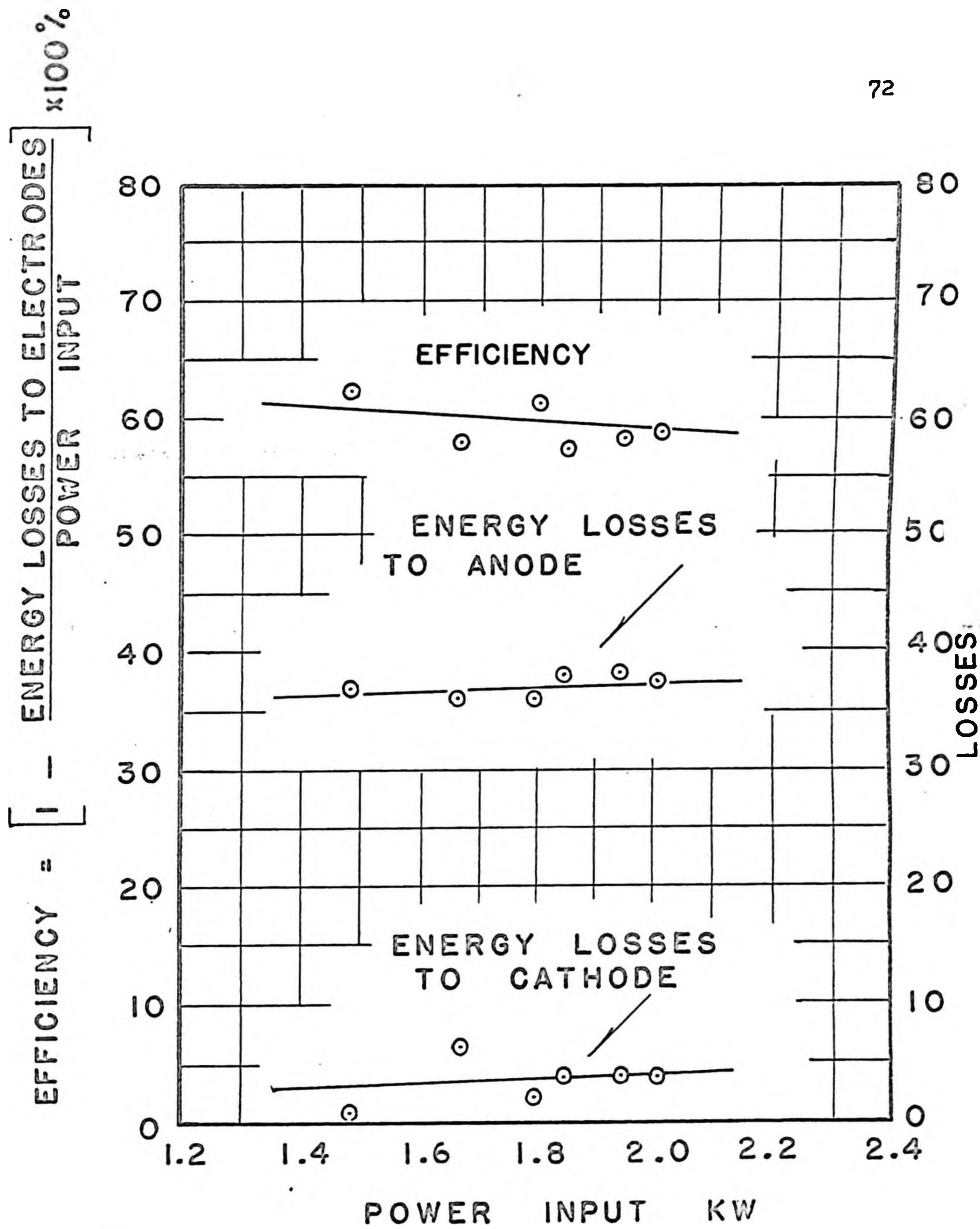

FIG.12 EFFICIENCY OF THE PLASMA GENERATOR – COPPER ANODE GRAPHITE CATHODE ARGON 122 GM./MIN.

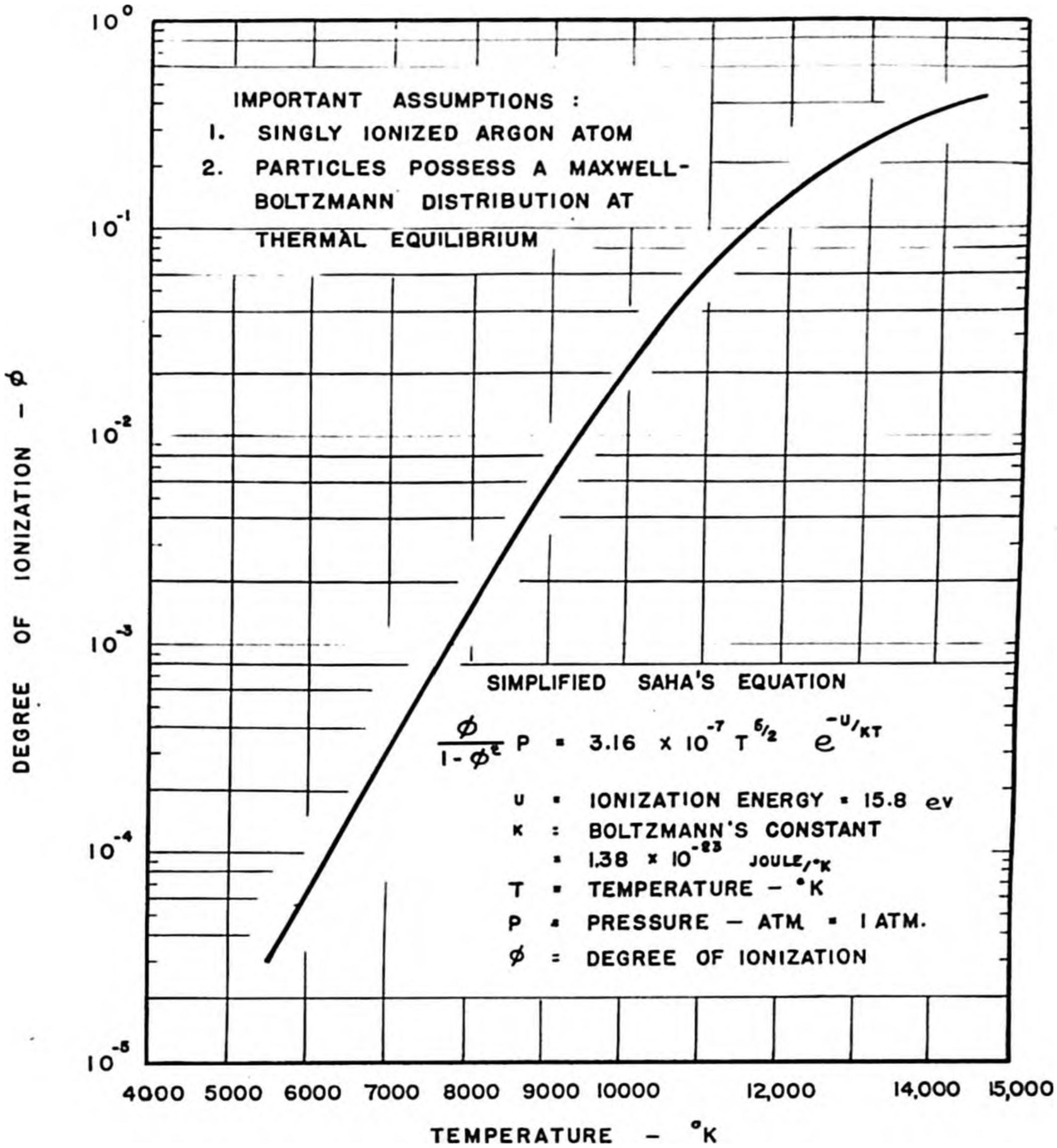

FIG. 13 DEGREE OF IONIZATION OF ARGON AT ATMOSPHERIC PRESSURE

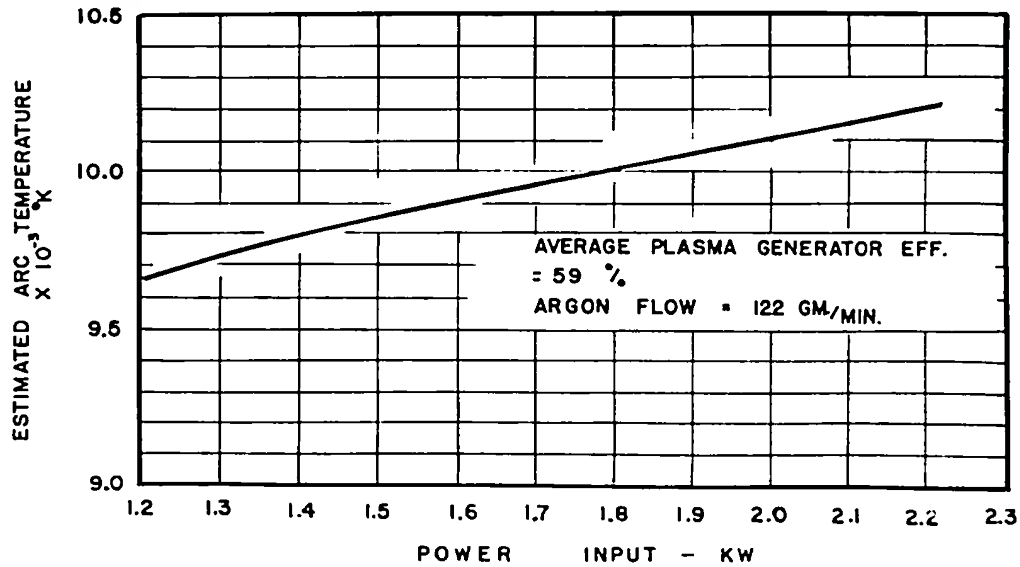

FIG. 14 ESTIMATED PLASMA ARC TEMPERATURE AS A FUNCTION OF POWER INPUT

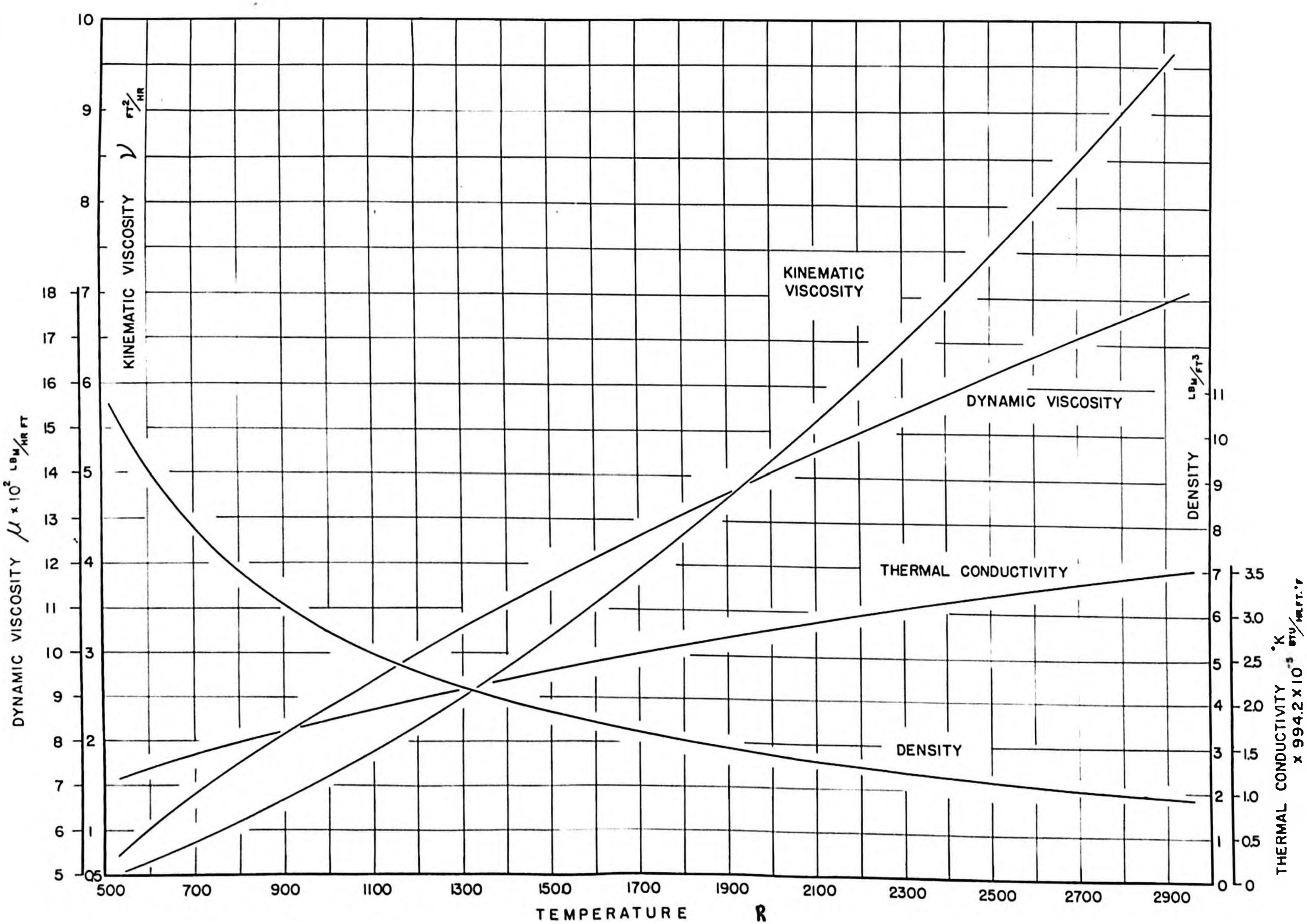

FIG. 15 PHYSICAL PROPERTIES OF ARGON AT ATMOSPHERIC PRESSURE

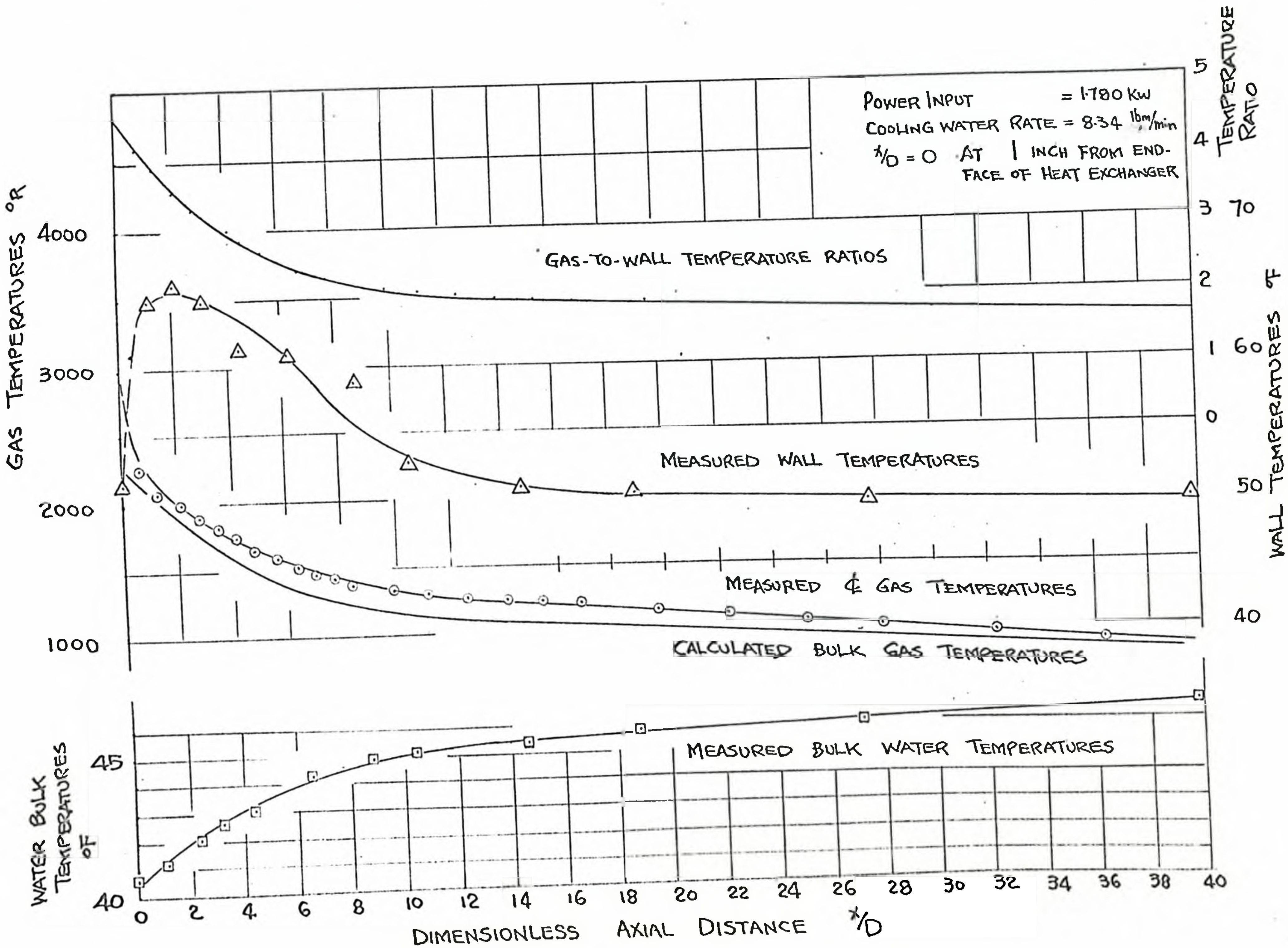

FIGURE 16a LONGITUDINAL TEMPERATURE VARIATIONS

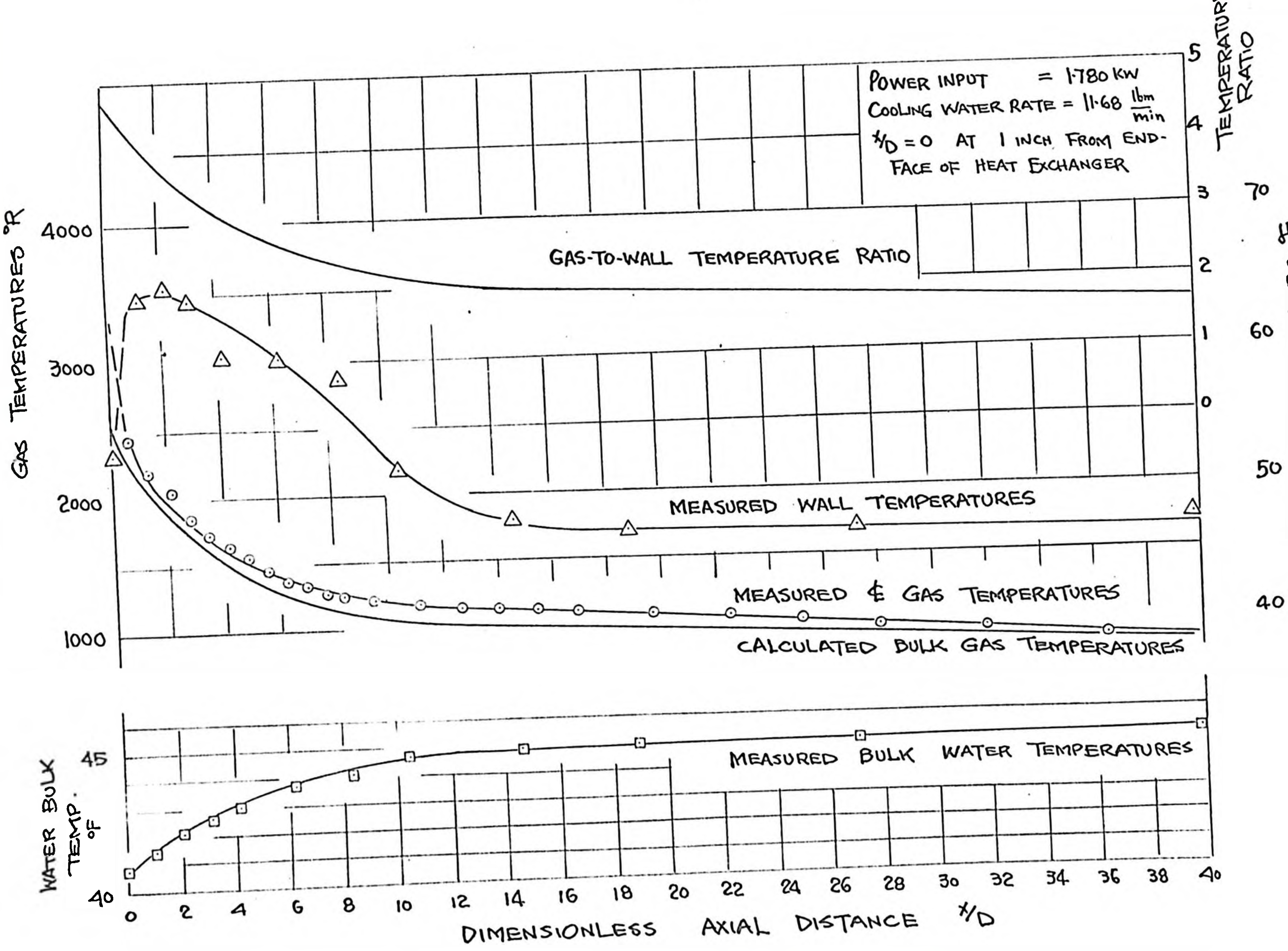

FIGURE 16b LONGITUDINAL TEMPERATURE VARIATIONS

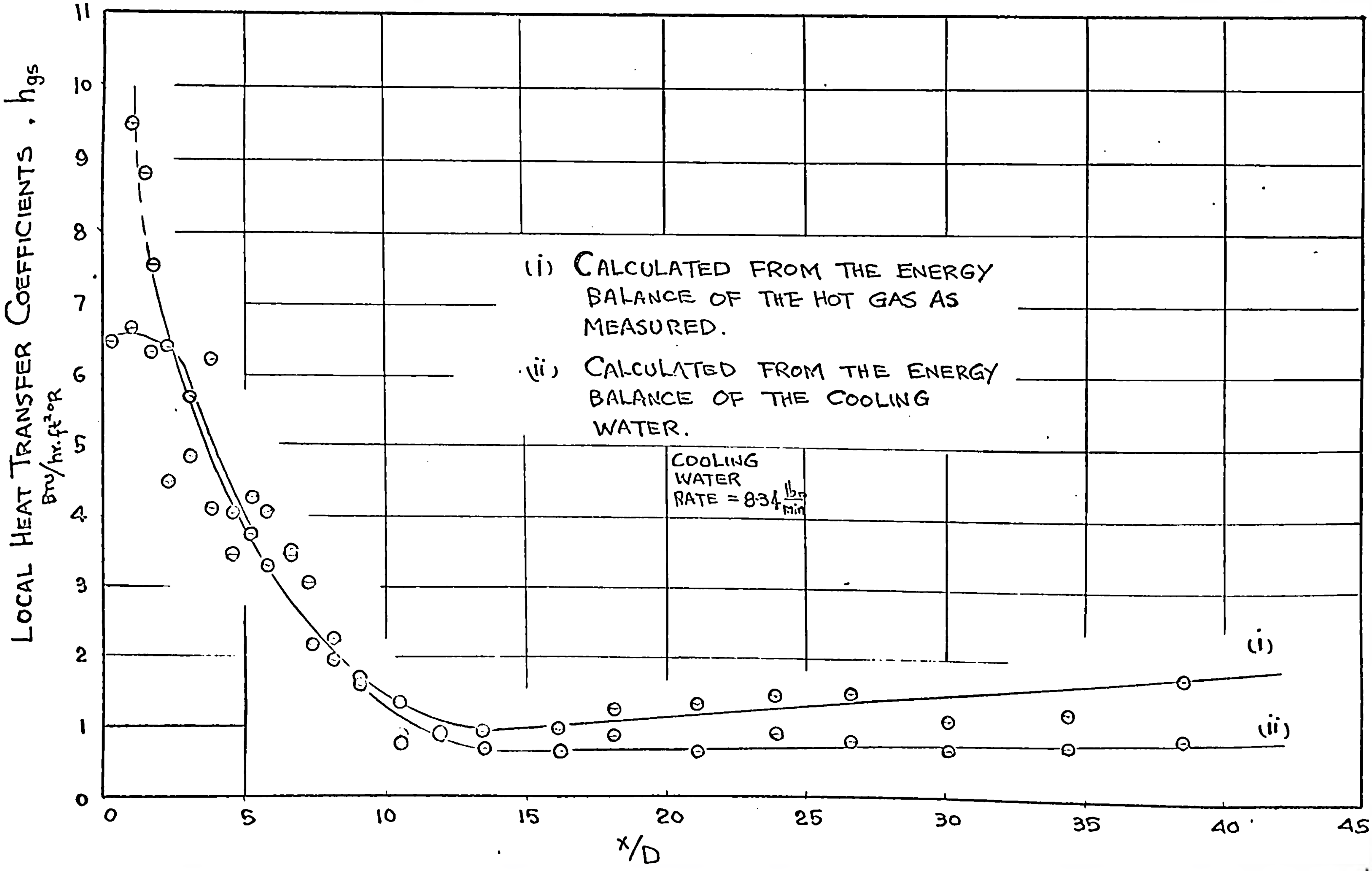

FIGURE 17a. LOCAL HEAT TRANSFER COEFFICIENTS AS A FUNCTION OF AXIAL DISTANCE

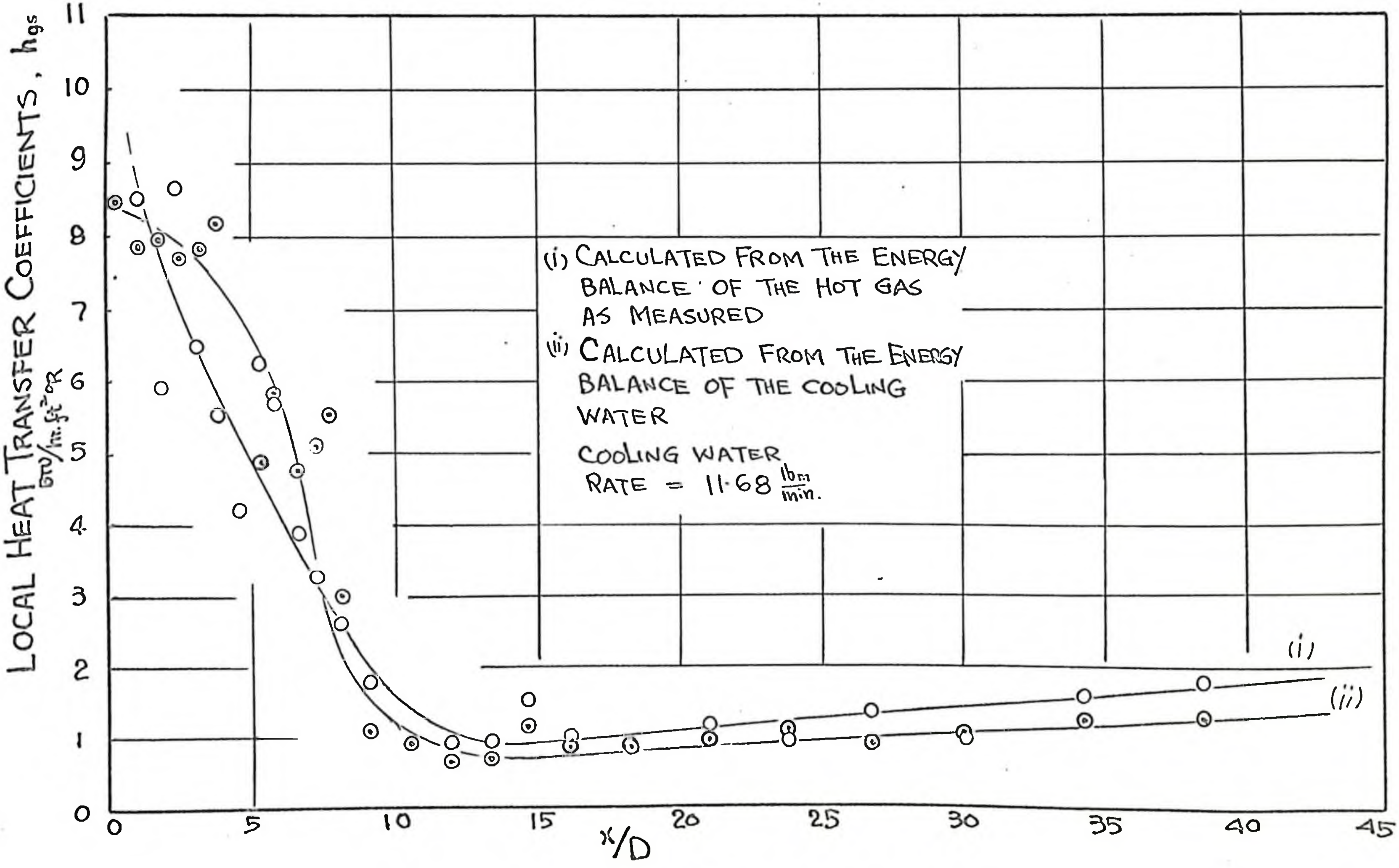

FIGURE 17b LOCAL HEAT TRANSFER COEFFICIENTS AS A FUNCTION OF AXIAL DISTANCE

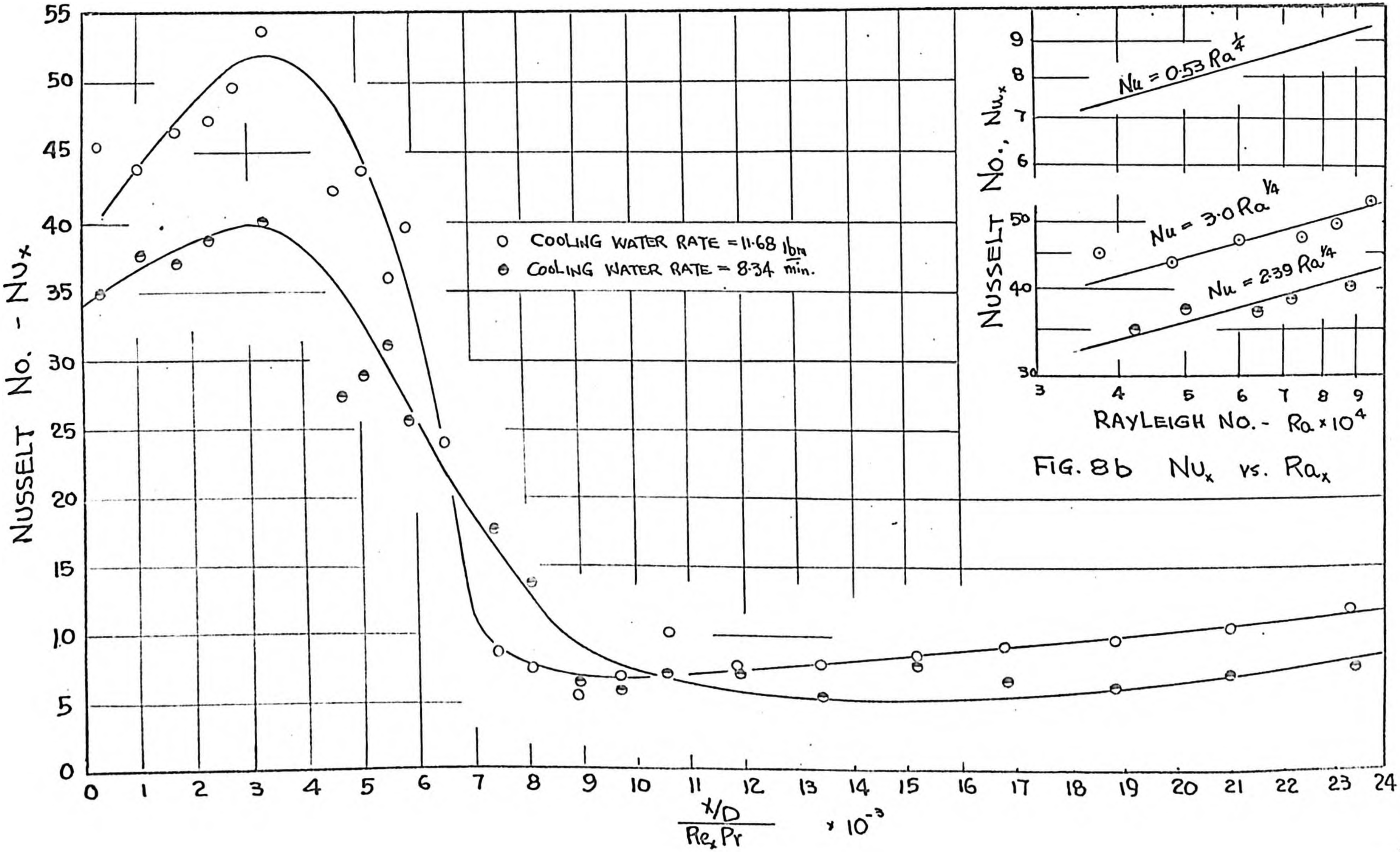

FIGURE 18a NUSSFIT NO. AS A FUNCTION OF NONDIMENSIONAL LENGTH

A P P E N D I X

TABLE A.1 TEMPERATURE MEASUREMENTS

1 Power Input = 1.780 kw
Gas Flow = .2593 lbm/min
Cooling Water Rate = 8.34 lbm/min

MEASUREMENT OF WALL AND WATER BULK TEMPERATURES

X/D	WALL TEMPERATURES TOP MV	BOT. MV	AVG. MV	TEMP. °F	WATER BULK TEMPERATURES TOP MV	BOT. MV	AVG. MV	TEMP. °F
0	0.450	0.416	.433	52.0	0.195	0.173	0.184	40.6
1.05	0.850	0.590	.720	65.0	0.200	0.194	0.197	41.2
2.10	0.780	0.706	.743	66.0	0.250	0.178	0.214	42.0
3.15	0.760	0.716	.738	65.4	0.257	0.203	0.230	42.7
4.20	0.700	0.561	.630	61.0	0.260	0.212	0.236	43.0
6.30	0.640	0.597	.613	60.2	0.272	0.262	0.267	44.4
8.40	0.600	0.550	.575	58.5	0.283	0.273	0.278	44.9
10.50	0.530	0.352	.441	52.4	0.290	0.274	0.282	45.1
14.70	0.465	0.357	.411	51.0	0.291	0.287	0.289	45.4
18.90	0.410	0.393	.401	50.6	0.294	0.296	0.295	45.7
27.30	0.382	0.354	.368	50.0	0.299	0.313	0.301	46.0
39.80	0.368	0.367	.366	48.9	0.313	0.317	0.315	46.6

MEASUREMENT OF GAS BULK TEMPERATURES

X/D	MV	TEMP.	X/D	MV	TEMP.	X/D	MV	TEMP.
0	52.0	2350	6.3	16.40	750	16.8	12.40	580
.70	33.70	1490	7.0	15.40	710	19.6	11.50	540
1.40	31.70	1400	7.7	15.60	720	22.4	10.00	480
2.10	30.50	1340	8.4	15.40	710	25.2	9.00	430
2.80	25.80	1150	9.8	14.00	650	28.0	9.10	435
3.50	23.20	1040	11.2	13.80	640	32.2	9.40	450
4.20	23.50	1050	12.6	13.0	610	36.4	8.50	410
4.90	20.10	910	14.0	12.80	600	40.6	7.90	380
5.60	18.50	840	15.4	12.60	590			

TABLE A.1 (continued)

2 Power Input = 1.780 kw
Gas Flow = 0.2593 lbm/min
Cooling Water Rate = 11.68 lbm/min

MEASUREMENT OF WALL AND WATER BULK TEMPERATURES

X/D	WALL TEMPERATURES TOP MV	BOT. MV	AVG. MV	TEMP. ^{o}F	WATER BULK TEMPERATURES TOP MV	BOT. MV	AVG. MV	TEMP. ^{o}F
0	0.50	0.44	0.470	53.7	0.190	0.188	0.189	40.8
1.05	0.710	0.706	0.708	64.5	0.208	0.200	0.204	41.5
2.10	0.730	0.718	0.724	65.2	0.224	0.208	0.216	42.1
3.15	0.720	0.694	0.707	64.4	0.230	0.226	0.228	42.6
4.20	0.640	0.600	0.620	60.5	0.240	0.232	0.236	43.0
6.30	0.620	0.610	0.615	60.3	0.258	0.244	0.251	43.70
8.40	0.340	0.310	0.325	57.0	0.262	0.258	0.260	44.10
10.50	0.220	0.210	0.215	52.0	0.272	0.274	0.273	44.70
14.70	0.340	0.338	0.339	47.7	0.276	0.276	0.276	44.80
18.90	0.320	0.320	0.320	46.8	0.275	0.277	0.276	44.82
27.30	0.328	0.330	0.329	47.2	0.278	0.278	0.278	44.90
39.80	0.334	0.332	0.333	47.4	0.279	0.281	0.280	45.03

MEASUREMENT OF GAS BULK TEMPERATURES

X/D	MV	TEMP.	X/D	MV	TEMP.	X/D	MV	TEMP.
0	49.0	2200	6.3	15.50	715	16.8	12.0	560
.70	33.8	1495	7.0	15.70	720	19.6	11.5	540
1.40	30.60	1355	7.7	16.5	755	22.4	10.5	495
2.1	27.8	1235	8.4	15.5	715	25.2	8.6	410
2.8	24.5	1095	9.8	14.5	670	28.0	8.0	385
3.5	22.5	1010	11.2	13.6	630	32.2	8.0	385
4.2	22.5	1010	12.6	13.0	605	36.4	7.8	375
4.9	20.0	905	14.0	12.9	600	40.6	7.6	370
5.6	16.4	750	15.4	12.9	600			

TABLE A.1 (continued)

3 Power Input = 1.780 kw
Gas Flow = .2593 lbm/min
Cooling Water Rate = 10.53 lbm/min

MEASUREMENT OF WALL AND WATER BULK TEMPERATURES

	WALL TEMPERATURES				WATER BULK TEMPERATURES			
X/D	TOP MV	BOT. MV	AVG. MV	TEMP. °F	TOP MV	BOT. MV	AVG. MV	TEMP. °F
0	0.388	0.410	0.389	50.0	0.184	0.190	0.187	40.7
1.05	0.622	0.640	0.631	61.0	0.200	0.204	0.202	41.4
2.10	0.686	0.688	0.687	63.5	0.227	0.229	0.228	42.6
3.15	0.634	0.650	0.642	61.5	0.231	0.235	0.243	42.8
4.20	0.610	0.622	0.616	60.3	0.242	0.244	0.243	43.3
6.30	0.788	0.790	0.789	68.1	0.256	0.260	0.258	44.0
8.40	0.456	0.454	0.455	53.0	0.261	0.265	0.263	44.2
10.50	0.379	0.380	0.378	49.5	0.264	0.270	0.233	44.4
14.70	0.354	0.360	0.357	48.5	0.272	0.270	0.271	44.6
18.90	0.334	0.340	0.337	47.3	0.278	0.272	0.275	44.8
27.30	0.350	0.360	0.355	48.2	0.240	0.276	0.278	44.9
39.80	0.352	0.360	0.356	47.7	0.292	0.294	0.293	45.6

MEASUREMENT OF GAS BULK TEMPERATURES

X/D	MV	TEMP.	X/D	MV	TEMP.	X/D	MV	TEMP.
0	48.0	2150	6.3	18.5	840	16.8	12.1	570
0.7	32.8	1450	7.0	17.0	780	19.6	11.7	550
1.4	32.0	1420	7.7	15.6	720	22.4	11.9	560
2.1	30.5	1360	8.4	14.7	680	25.2	11.5	540
2.8	27.0	1200	9.8	14.0	650	28.0	10.1	480
3.5	24.6	1100	11.2	13.5	630	32.2	8.7	420
4.2	23.5	1050	12.6	12.5	590	36.4	9.2	440
4.9	23.5	1050	14.0	12.5	590	40.6	8.1	390
5.6	20.4	920	15.4	13.0	610			

TABLE A.1 (continued)

4 Power Input = 1.730 kw
Gas Flow = .2593 lbm/min
Cooling Water Rate = 16.72 lbm/min

MEASUREMENT OF WALL AND WATER BULK TEMPERATURES

X/D	WALL TEMPERATURES TOP MV	BOT. MV	AVG. MV	TEMP. °F	WATER BULK TEMPERATURES TOP MV	BOT. MV	AVG. MV	TEMP. °F
0	0.196	0.194	0.195	41.1	0.187	0.185	0.186	40.7
1.05	0.450	0.350	0.400	50.5	0.205	0.207	0.206	41.0
2.10	0.440	0.360	0.400	50.5	0.210	0.220	0.215	42.0
3.15	0.420	0.398	0.409	50.9	0.216	0.212	0.214	42.1
4.20	0.410	0.390	0.400	50.5	0.220	0.210	0.230	42.7
6.30	0.362	0.356	0.359	48.6	0.240	0.232	0.236	43.0
8.40	0.360	0.340	0.350	48.2	0.241	0.241	0.241	43.2
10.50	0.352	0.344	0.348	48.1	0.244	0.246	0.245	43.4
14.70	0.252	0.246	0.249	43.6	0.246	0.248	0.247	43.5
18.90	0.270	0.268	0.269	44.5	0.248	0.250	0.249	43.6
27.30	0.268	0.262	0.265	44.3	0.250	0.254	0.252	43.7
39.80	0.264	0.260	0.262	44.1	0.258	0.258	0.258	44.0

MEASUREMENT OF GAS BULK TEMPERATURES

X/D	MV	TEMP.	X/D	MV	TEMP.	X/D	MV	TEMP.
0	46.0	2050	6.3	15.2	700	16.8	8.5	410
.7	31.6	1400	7.0	14.0	650	19.6	8.3	400
1.4	30.5	1350	7.7	13.3	620	22.4	8.1	390
2.1	38.6	1270	8.4	12.4	580	25.2	7.2	350
2.8	26.0	1160	9.8	11.7	550	28.0	6.8	330
3.5	23.0	1040	11.2	12.0	560	32.2	6.3	310
4.2	21.0	950	12.6	11.5	540	36.4	5.6	280
4.9	19.0	860	14.0	10.1	480	40.6	5.2	260
5.6	15.5	710	15.4	9.4	450			

TABLE A.2.1
CALCULATED RESULTS ON HEAT TRANSFER FROM HOT GAS

AXIAL POSITION X/D	WATER BULK TEMPERATURES FROM GRAPH °F	BULK TEMP. RISE °F	ENERGY BALANCE OF COOLING WATER BTU/MIN	BULK TEMP. RISE OF HOT GAS (CAL.) °R	CORRECTED GAS TEMPERATURE °R	BULK TEMP. RISE OF HOT GAS (MEA.) °R
0	40.40	0.70	5.84	182	-	-
0.7	41.10	0.65	5.42	168	2470	280
1.4	41.75	0.55	4.59	143	2190	190
2.1	42.30	0.50	4.17	135	2000	100
2.8	42.80	0.40	3.34	106	1900	100
3.5	43.20	0.40	3.34	106	1800	80
4.2	43.60	0.20	1.67	52	1720	70
4.9	43.80	0.20	1.67	52	1650	70
5.6	44.00	0.20	1.67	52	1580	60
6.3	44.20	0.20	1.67	52	1520	50
7.0	44.40	0.20	1.67	52	1470	50
7.7	44.60	0.15	1.25	39	1420	30
8.4	44.75	0.25	2.09	65	1390	50
9.8	45.00	0.18	1.50	47	1340	40
11.2	45.18	0.12	1.00	31	1300	30
12.6	45.30	0.05	0.42	13	1270	20
14.0	45.35	0.05	0.42	13	1250	20
15.4	45.40	0.05	0.42	13	1240	10
16.8	45.45	0.10	0.83	26	1200	40
19.6	45.55	0.07	0.58	18	1150	50
22.4	45.62	0.10	0.83	26	1100	50
25.2	45.72	0.08	0.67	21	1050	50
28.0	45.80	0.10	0.83	25	1000	50
32.2	45.90	0.10	0.83	26	950	50
36.4	46.00	0.10	0.83	26	900	63
40.6	46.10				837	
			47.50 BTU/min.			

Arc power input = 1.780 kw.

Cooling water rate = 8.34 lb./min.

TABLE A.2.1 (continued)

ENERGY BALANCE OF HOT GAS	MEAN BULK GAS TEMP. BASED ON THE ENERGY BALANCE OF COOLING WATER	MEASURED WALL TEMPS.	GAS-TO-WALL TEMPERATURE RATIOS	LOCAL HEAT TRANSFER COEFFICIENTS BASED ON THE ENERGY BALANCE OF THE COOLING WATER	HOT GAS
BTU/MIN	^oR	^oR		BTU/hrft^{2o}R	
-	2373	512	4.64	6.45	-
9.0	2191	523	4.19	6.63	9.50
6.11	2023	525	3.88	6.30	7.53
3.22	1875	525	3.58	6.35	4.43
2.57	1740	526	3.35	5.67	4.81
2.25	1634	525	3.18	6.2	4.14
2.25	1476	524	3.01	3.42	4.03
1.93	1423	523	2.87	3.68	4.23
1.61	1371	519	2.64	4.03	3.30
1.61	1319	518	2.54	4.28	3.47
.96	1267	517	2.45	3.43	2.18
1.61	1215	516	2.35	3.08	1.89
1.29	1176	514	2.29	2.33	1.60
.96	1111	512	2.17	1.72	1.26
.64	1064	511	2.08	.78	.86
.64	1032	511	2.02	.83	.89
.32	1019	511	1.99	.85	.45
1.29	1006	511	1.97	.86	.96
1.61	993	511	1.94	.62	1.29
1.61	967	511	1.89	.93	1.38
1.61	949	511	1.86	.78	1.53
1.61	923	510	1.81	.69	1.12
1.61	876	510	1.72	.78	1.25
2.03	850	510	1.67	.84	1.78

52.50 BTU/min

TABLE A.2.1 (continued)

GAS FILM TEMP. °R	THERMAL COND. BTU/hr.ft.°R $k \times 994 \times 10^{-5}$	DYNAMIC VISCOSITY lbm/hr.ft. $\mu \times 10^{-2}$	KINEMATIC VISCOSITY ft²/hr. ν	NUSSELT NUMBER $\frac{hD}{k}$	REYNOLD NUMBER $\frac{mD}{A\mu}$	GRASHOF NUMBER $\frac{g\beta\Delta TD^3}{\nu^2} \times 10^4$	$\frac{x/D}{Re_x Pr} \times 10^{-3}$
1442	2.20	11.30	2.95	35.0	1470	6.36	.36
1357	2.11	10.82	2.66	37.6	1540	7.60	1.03
1274	2.03	10.38	2.40	37.0	1600	9.80	1.66
1201	1.96	10.00	2.16	38.7	1660	10.90	2.23
1143	1.90	9.63	2.00	35.6	1730	12.35	2.75
1097	1.85	9.38	1.86	40.0	1780	13.95	3.27
1051	1.80	9.10	1.75	22.7	1830	15.40	3.76
1012	1.75	8.86	1.65	25.1	1870	16.90	4.24
972	1.70	8.62	1.53	27.1	1920	19.10	4.69
945	1.68	8.42	1.45	28.6	1970	20.90	5.10
918	1.64	8.28	1.39	31.1	2010	22.30	5.53
892	1.61	8.10	1.32	25.4	2050	24.0	5.94
865	1.57	7.92	1.25	23.4	2100		6.54
845	1.55	7.80	1.20	17.9	2130		7.45
811	1.50	7.56	1.12	13.6	2200		8.18
787	1.45	7.40	1.05	6.4	2250		8.93
771	1.43	7.30	1.03	6.9	2280		9.75
765	1.42	7.25	1.00	7.1	2290		10.64
758	1.41	7.20	0.99	7.2	2310		11.90
752	1.40	7.15	0.98	5.3	2320		13.70
739	1.38	7.02	0.94	8.0	2370		15.20
730	1.37	7.00	0.92	6.8	2380		16.80
716	1.36	6.90	0.90	6.1	2410		18.90
693	1.31	6.72	0.85	7.1	2410		21.00
680	1.28	6.65	0.80	7.8	2500		23.30

TABLE A.2.2
CALCULATED RESULTS ON HEAT TRANSFER FROM HOT GAS

AXIAL POSITION	MEASURED WATER BULK TEMP.	TEMP. RISE	ENERGY BALANCE OF WATER	MEASURED GAS TEMP.	TEMP. RISE	ENERGY BALANCE OF HOT GAS
X/D	°F	°F	BTU/MIN	°R	°R	BTU/MIN
0.0	40.40	.70	8.17	–	–	–
0.7	41.10	.57	6.65	2450	250	8.05
1.4	41.67	.51	5.95	2200	150	4.82
2.1	42.18	.44	5.14	2050	200	6.45
2.8	42.62	.40	4.66	1850	130	4.18
3.5	43.02	.37	4.32	1720	100	3.22
4.2	43.39	.13	1.52	1620	70	2.25
4.9	43.52	.18	2.10	1550	100	3.22
5.6	43.70	.20	2.34	1450	80	2.58
6.3	43.90	.15	1.75	1370	50	1.61
7.0	44.05	.15	1.75	1320	40	1.29
7.7	44.20	.15	1.75	1280	30	0.97
8.4	44.35	.15	1.75	1250	40	1.29
9.8	44.50	.05	.58	1210	20	0.64
11.2	44.55	.04	.47	1190	20	0.64
12.6	44.59	.03	.35	1170	20	0.64
14.0	44.62	.03	.35	1150	30	0.97
15.4	44.65	.05	.58	1120	20	0.64
16.8	44.70	.07	.82	1100	30	0.97
19.6	44.77	.07	.82	1070	40	1.29
22.4	44.84	.07	.82	1030	30	0.97
25.2	44.91	.07	.82	1000	40	1.29
28.0	44.98	.10	1.17	960	40	1.29
32.2	45.08	.10	1.17	920	60	1.93
36.4	45.18	.10	1.17	860	60	1.93
40.6	45.28			800		
			57.0 BTU/min.			53.90 BTU/min.

Arc power input = 1.78 kw
Cooling water rate= 11.68 lb./min.

TABLE A.2.2 (continued)

CALCULATED GAS TEMP. RISE °R	CALCULATED GAS TEMP. °R	MEASURED WALL TEMP. °R	TEMP. RATIO	LOCAL HEAT TRANSFER COEFFICIENTS BASED ON THE ENERGY BALANCE OF THE COOLING WATER BTU/hrft^2°R	HOT GAS BTU/hrft^2°R
257	2495	514	4.86	8.50	–
207	2265	524	4.32	7.85	8.58
185	2069	525	3.96	7.92	5.92
160	1897	525	3.62	7.70	8.67
145	1745	525	3.32	7.85	6.48
135	1605	524	3.06	8.20	5.53
47	1464	523	2.82	3.51	4.22
65	1408	522	2.70	4.87	6.44
73	1340	520	2.55	5.86	5.71
55	1276	519	2.42	4.75	3.89
55	1221	517	2.34	5.10	3.31
55	1166	515	2.26	5.52	2.61
55	1111	512	2.16	3.00	1.80
18	1072	510	2.08	1.06	0.94
15	1053	509	2.06	0.89	0.97
11	1043	508	2.04	.68	.99
11	1032	508	2.03	.69	1.55
18	1017	508	2.01	1.18	1.07
25	995	508	1.95	.87	.84
25	970	508	1.91	.91	1.13
25	945	508	1.86	.96	.96
25	920	508	1.81	1.02	1.35
36	890	508	1.75	1.05	.93
36	854	508	1.68	1.16	1.60
36	818	508	1.61	1.29	1.80

TABLE A.2.2. (continued)

GAS FILM TEMP. °R	THERMAL COND. BTU/hr.ft°R $k \times 9940 \times 10^{-5}$	DYNAMIC VISCOSITY lbm/hr.ft. $\mu \times 10^{-2}$	KINEMATIC VISCOSITY ft²/hr ν	NUSSELT NUMBER $\frac{hD}{k}$	REYNOLD NUMBER $\frac{\dot{m}D}{A\mu}$	GRASHOF NUMBER $\frac{g\beta\Delta T D^3}{\nu^2} \times 10^4$	$\frac{x/D}{Re_x Pr}$ $\times 10^{-3}$
1528	2.23	11.52	3.13	45.4	1445	5.64	.368
1406	2.13	10.95	2.73	43.9	1520	7.24	1.044
1303	2.03	10.40	2.40	46.4	1600	9.10	1.652
1210	1.95	9.92	2.15	47.1	1680	11.35	2.20
1130	1.88	9.60	1.96	49.7	1730	12.85	2.75
1055	1.83	9.28	1.83	53.4	1790	14.30	3.25
990	1.77	8.94	1.67	(22.3)	1860	16.70	3.70
967	1.70	8.60	1.52	34.2	1940	19.30	4.09
945	1.65	8.32	1.40	42.3	2000	21.90	4.50
896	1.61	8.10	1.34	43.5	2050	23.30	4.90
868	1.57	7.95	1.25	36.0	2090	26.00	5.32
844	1.53	7.80	1.20	39.7	2140	27.80	5.68
816	1.50	7.60	1.13	23.8	2190	-	6.28
792	1.47	7.42	1.07	8.7	2240	-	7.09
782	1.45	7.35	1.05	7.3	2260	-	7.95
775	1.44	7.30	1.03	5.7	2280	-	8.81
770	1.42	7.28	1.02	5.8	2290	-	9.59
762	1.41	7.24	1.00	10.0	2300	-	10.58
751	1.40	7.15	0.98	7.5	2330	-	11.82
739	1.37	6.95	0.95	8.0	2400	-	13.21
726	1.36	6.90	0.90	8.4	2410	-	14.9
714	1.34	6.85	0.88	9.1	2430	-	16.6
699	1.20	6.78	0.85	9.7	2450	-	18.6
681	1.28	6.65	0.83	10.7	2500	-	20.7
663	1.26	6.50	0.78	12.2	2530	-	23.0

TABLE A.3
MEASURED AND CALCULATED RESULTS ON PLASMA GENERATOR CHARACTERISTICS

Voltage-Current Relation

Constant Transpiration Fluid Flow Rate = 122 gm/min

Average Arc Voltage, volts:	20.5	22	21.3	21	22	23	23	22.5
Average Arc Current, amperes:	70	74	75	80	83	85	87	95

Effect of Gas Flow Rate on Arc Voltage

Constant Arc Current = 70 amperes

Average Arc Voltage, volts:	13	12	13	16	21	22	24	25
Gas Flow Rate, gm./min. :	67	75	90	110	122	135	160	170

Estimated Temperatures of the Plasma Arc

Average Efficiency of the Plasma Generator = 59%

Arc Power Input, kw	1.2	1.5	1.7	2.1	2.3	2.5
Degree of Ionization, $\phi \times 10^{-2}$	1.550	1.938	2.193	2.710	2.870	3.225
Arc Temperatures, $^{\circ}K$	9700	9900	10,000	10,200	10,250	10,350

TABLE A.3 (continued)

AVERAGE ARC VOLTAGE	AVERAGE ARC CURRENT	AVERAGE POWER INPUT	COOLING WATER RATE AT ANODE	COOLING WATER RATE AT CATHODE	INLET WATER TEMPERATURE
VOLTS	AMPERES	KW.	lbm/min	lbm/min	°F
20	75	1.496	2.66	21.07	41.50
20.5	81	1.660	2.66	21.07	41.00
21.5	83	1.794	2.66	21.07	40.80
20.5	90	1.845	2.66	21.07	40.50
22	88	1.940	2.66	21.07	41.50
23	87	2.00	2.66	21.07	41.30

OUTLET TEMP. OF ANODE COOLING WATER	OUTLET TEMP. OF CATHODE COOLING WATER	ENERGY LOSSES TO ELECTRODES	APPROXIMATE ENERGY TRANSFER EFFICIENCY	ENTHALPY OF EMERGING PLASMA JET	CATHODE EROSION RATE
°F	°F	BTU/min	%	KCal/gm-mole	gm/min.
53.30	0	31.40	63%	4.42	0.0110
55.10	41.10	39.60	58.0%	4.52	0.0108
54.50	40.90	38.61	62.0%	5.22	0.0112
55.65	40.70	42.41	59.5%	5.17	0.0115
57.25	41.70	46.11	58.2%	5.30	0.0116
57.35	41.50	46.91	58.8%	5.54	0.0130

Constant Transpiration Fluid Flow Rate = 122. GM/MIN.
Constant Arc Gap Distance = 1/16 inch

APPENDIX B

Sample Calculations

1. Energy losses to the electrodes

Heat gained by the anode cooling water

= anode cooling water rate specific heat of water

water outlet temperature - water inlet temperature

$\therefore Q_{wa} = m_{wa} C_{pw} (t_2 - t_1)$

$= 2.66 \ lb_m/min \ \ 1 \ BTU/lb_m{}^{o}F \ (57.35 - 41.30)^{o}F$

$= \underline{42.70 \ BTU/min.}$

Heat gained by the cathode cooling water

= cathode cooling water rate specific heat of water

water outlet temperature - water inlet temperature

$\therefore Q_{wc} = m_{wc} C_{pw} (t_3 - t_1)$

$= 21.07 \ lb_m/min \ \ 1 \ BTU/lb_m{}^{o}F \ (41.50 - 41.30)^{o}F$

$= \underline{4.21 \ BTU/min.}$

Heat lost by radiation at the anode

= (emissivity of copper) x (Stefan-Boltzmann's constant)

x (Absolute temperature of the anode)^4 x (anode area in contact with the plasma arc)

$\therefore Q_{ra} = \epsilon_c \sigma T_a{}^4 A_a$

$= (0.77)\ (0.1714 \times 10^{-8}) \dfrac{BTU}{hr.ft^2\ {}^{o}R^4}\ (2440)^4\ {}^{o}R^4\ (\pi \times \dfrac{0.625}{144} \times 0.5)\ ft^2$

$= 32.1\ \dfrac{BTU}{hr}$

$= \underline{0.535 \text{ BTU/min.}}$

$$\frac{Q_{ra}}{Q_{wa}} = \frac{0.535}{42.70} \times 100\% = 1.2\% \text{ (negligible)}$$

2. Energy transfer efficiency of the plasma generator

$$= \left\{1 - \left[\frac{\text{Energy losses to electrodes}}{\text{Arc power input}}\right]\right\} \times 100\%$$

$$= \left\{1 - \left[\frac{(42.70 + 4.21) \text{ BTU/min.}}{2.0 \text{ kw} \times 56.8 \text{ BTU/min/kw}}\right]\right\} \times 100\%$$

$= \underline{58.8\%}.$

3. Heat transfer rate at anode

$$= \frac{\text{Total heat transfer at anode}}{\text{Area of anode actually in contact with the plasma arc}}$$

$$\therefore \left(\frac{Q}{A}\right)_a = \frac{Q_{wa}}{A_a}$$

$$= \frac{42.70 \frac{\text{BTU}}{\text{min}} \times 60 \frac{\text{min}}{\text{hr}}}{\frac{\pi \times 0.625 \times 0.5 \text{ ft}^2}{144}}$$

$= \underline{375{,}000 \text{ BTU/hr.}}$

4. Degree of ionization

$$= \frac{\text{No. of ionized particles}}{\text{No. of neutral atoms}}$$

$$\therefore \phi = \frac{\eta P/u_I}{M_g N}$$

$$= \frac{0.588 \times 2.0 \text{ kw} \times 1000 \text{ joules/sec/kw}}{15.8 \text{ ev} \times 1.602 \times 10^{-19} \text{ joules/ion/ev}}$$

$$\times 122 \frac{\text{gm}}{\text{min}} \cdot \frac{1}{60} \frac{\text{min}}{\text{sec}} \frac{1}{10^3} \frac{\text{kg}}{\text{gm}} \frac{1}{39.944} \text{ mole}$$

$$\times 6.0251 \times 10^{26} \frac{\text{particles}}{\text{kg-mole}}$$

$= \underline{0.02582}$

5. Temperature of the plasma arc is found directly from Figure 13, after ϕ is obtained in 4.

6. The average convective heat transfer coefficient at the thermocouple hot junction.

The correlation of Nusselt number and Reynolds number is given by

$$\frac{h_{gt} d_t}{k_{gc}} = 0.615 \left(\frac{m_g D_e}{A_c \mu_{gc}} \right)^{0.466}$$

d_t = 1/32 inch

m_g = 0.2593 lb_m/min.

D_e = .1192 ft.

A_c = .0112 ft^2

At a given apparent gas temperature measured by the thermocouple, k_{gc} and μ_{gc} can be obtained from Figure 15, and h_{gt} can be solved for.

For example, $T_{tx} = 1470^{\circ}R$

k_{gc} = 2.19 BTU/hr.ft$^{\circ}$R

μ_{gc} = 0.1155 lb_m/hr.ft.

$$\therefore h_{gt} = \frac{0.615}{\frac{1}{32}\frac{1}{12}\text{ ft}}\ 2.19 \frac{\text{BTU}}{\text{hr.ft}^{\circ}\text{R}} \left(\frac{0.2593 \frac{lb_m}{min} \times 60 \frac{min}{hr} \times 0.1192 \text{ ft}}{0.0112 \text{ ft}^2 \times 0.1155 \frac{lb_m}{hr.ft}} \right)^{0.466}$$

$$= 29.4 \frac{\text{BTU}}{\text{hr.ft}^{2\,\circ}\text{R}}$$

It was found after evaluating the local h_{gt} for the 26 positions along the tube axis, that it varied from about 30 to 19 BTU/hr.ft$^{2\,\circ}$F.

For convenience, an average value of h_{gt} was used in other temperature corrections.

7. Heat balance at thermocouple junction. The heat balance is given by:

$$\frac{q}{A_t} = h_{gt}\left(T - T_t\right)_x = \varepsilon_t \sigma \left(T_t^{\,4} - T_s^{\,4}\right)_x$$

where $h_{gt} = 29.4 \dfrac{\text{BTU}}{\text{hr.ft}^2\ {}^{\circ}\text{R}}$ (as found in 6.)

$T_t = 1470^{\circ}\text{R}$ (apparent gas temperature)

$\varepsilon_t = 0.8$ (for welded junction)

$\sigma = 0.1714 \times 10^{-8}\ \text{BTU/hr.ft}^2\ {}^{\circ}\text{R}^4$

$T_s = 550^{\circ}\text{R}$ (average wall temperature)

$$\therefore\ 29.4 \frac{\text{BTU}}{\text{hr.ft}^2\ {}^{\circ}\text{R}} \left(T - 1470\right)^{\circ}\text{R} = 0.8 \times 0.1714 \times 10^{-8} \frac{\text{BTU}}{\text{hr.ft}^2\ {}^{\circ}\text{R}^4}$$

$$\times\ (1470^4 - 550^4)^{\circ}\text{R}^4$$

$\therefore\ T_x$ = corrected gas temperature

$= \underline{1683^{\circ}\text{R.}}$

8. Energy balance of cooling water in the annular passage.

The energy balance is given by:

$$q_w = m_w\, C_{pw} \left(t_{x+\Delta x} - t_x\right)$$

For example, at $x/D = 10.50$

$$q_w = 11.68\ \text{lb}_m/\text{min} \times 1\ \text{BTU/lb}_m\,{}^{\circ}\text{F} \times \left(44.55 - 44.50\right)\,{}^{\circ}\text{F}$$

$= \underline{0.58\ \text{BTU/min.}}$

9. Energy balance of hot gas in the inner tube.

The energy balance is given by:

$$q_g = m_g C_{pg} \left(T_{x + \Delta x} - T_x\right)$$

For example, at x/D = 10.50

$$q_g = 0.2593 \text{ lb}_m/\text{min } 0.124 \text{ BTU/lb}_m {}^\circ\text{R} \left(1190 - 1210\right) {}^\circ\text{R}$$

$= \underline{-0.64 \text{ BTU/min}}$. The negative sign indicates that heat is being lost by the hot gas.

10. Estimation of gas temperatures based on the energy balance of the cooling water.

The expression is given by

$$-\left(T_{x + \Delta x} - T_x\right) = \frac{m_w C_{pw} \left(t_{x + \Delta x} - t_x\right)}{m_g C_{pg}}$$

Again at x/D = 10.50

$$-\left(T_{x + \Delta x} - T_x\right) = \frac{0.58 \text{ BTU/min}}{.0322 \text{ BTU/min} {}^\circ\text{R}}$$

$$= \underline{18^\circ\text{R}}.$$

Similarly, the temperature drops in the direction of the gas flow can be estimated. If the measured exhaust gas temperature is used as the estimated exit gas temperature, other temperatures of the gas can be found.

11. Evaluation of the local heat transfer coefficients.

(i) based on the heat balance of the cooling water

$$\therefore h_{gs} = \frac{m_w C_{pw} \left(t_{x + \Delta x} - t_x\right)}{A_i \left(T_{gb} - T_{gs}\right)}$$

In this case, $T_{gb} = \frac{1}{2}\left(T_{x + \Delta x} + T_x\right)$ calculated from 10.

At x/D = 10.50.

$$h_{gs} = \frac{0.58 \text{ BTU/min} \times 60 \text{ min/hr.}}{\frac{8.42}{144} \text{ ft}^2 \left(1072 - 512\right) {}^{o}\text{R}}$$

$$= \underline{1.07 \text{ BTU/hr.ft}^2 \, {}^{o}\text{R.}}$$

(ii) based on the heat balance of the hot gas

$$\therefore h_{gs} = \frac{0.64 \text{ BTU/min} \times 60 \text{ min/hr.}}{\frac{8.42}{144} \text{ ft}^2 \left(1200 - 512\right) {}^{o}\text{R}}$$

$$= \underline{0.94 \text{ BTU/hr.ft}^2 \, {}^{o}\text{R.}}$$

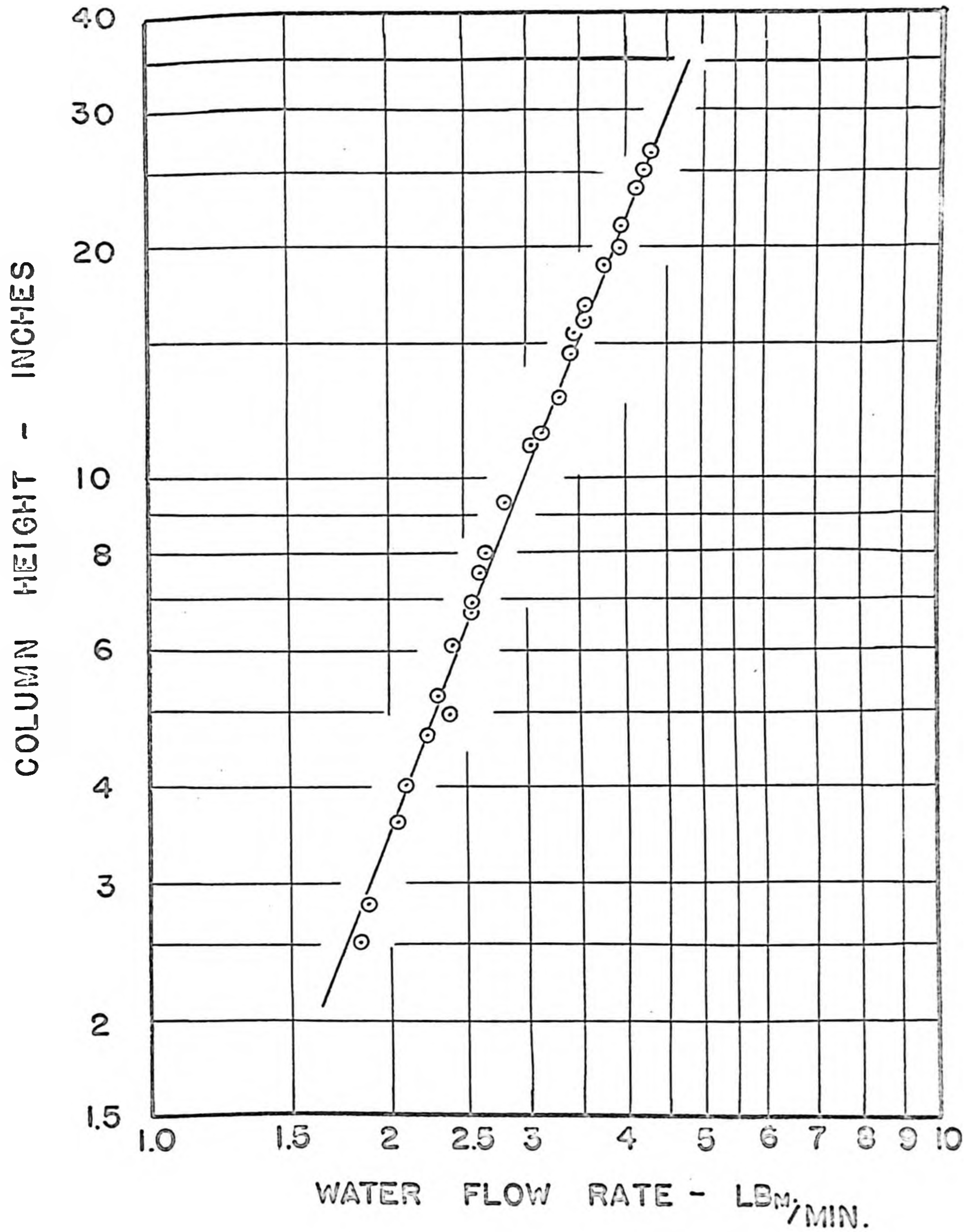

FIG.19 CALIBRATION CURVE - REYNOLDS COLUMN

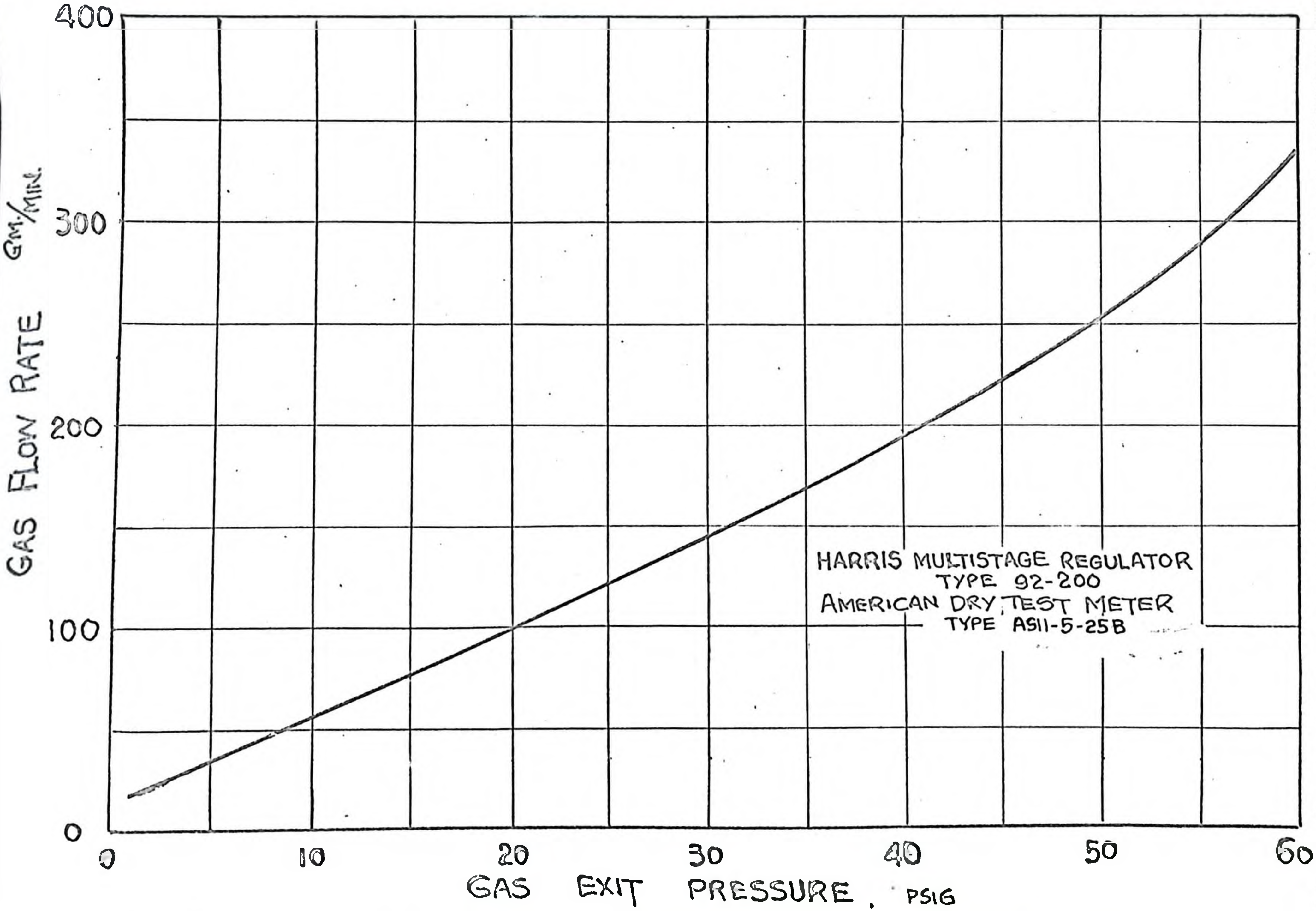

FIGURE 20 CALIBRATION CURVE FOR THE GAS METER

APPENDIX D

Estimation of the Temperature Drop Across the Wall of the Stainless Steel Tube

In a homogeneous body free of internal heat generation sources and with negligible axial conduction of heat in the wall, the rate of heat flow under steady state conditions, and the temperature drop across the tube wall can be related by the Fourier Law for Conduction. Therefore we have the following relation:

$$q = -kA \frac{dT}{dr} \qquad \text{(i)}$$

In the experiment, the teflon separators resting on the stainless steel tube acted as insulation to the heat flow. The area of heat flow then becomes $A = 2\pi\ell(r - \frac{c}{2\pi})$, where c is the total width of the teflon strips. Equation (i) is now rewritten as follows:

$$q = -k2\pi\ell(r - \frac{c}{2\pi}) \frac{dT}{dr}$$

$$dT = \frac{-q}{2\pi\ell k(r - \frac{c}{2\pi})} dr$$

$$\therefore \; T_i - T_o = \frac{q}{2\pi\ell k} \ln \frac{\frac{c}{2\pi} - r_o}{\frac{c}{2\pi} - r_i} \qquad \text{(ii)}$$

Consider the first six inches of the heat exchanger,

$$T_i - T_o = \frac{320 \frac{\text{BTU}}{\text{hr}} \ \ell n \frac{\frac{0.50}{2\pi} - 0.074}{\frac{0.50}{2\pi} - 0.715}}{2\pi \frac{1}{12} \text{ ft } 8.13 \frac{\text{BTU}}{\text{hr.ft}^{\circ}\text{F}}} = 2.9^{\circ}\text{F}$$